Spectroscopic, antimicrobial and computational study of novel benzoxazole derivative

Spectroscopic, antimicrobial and computational study of novel benzoxazole derivative

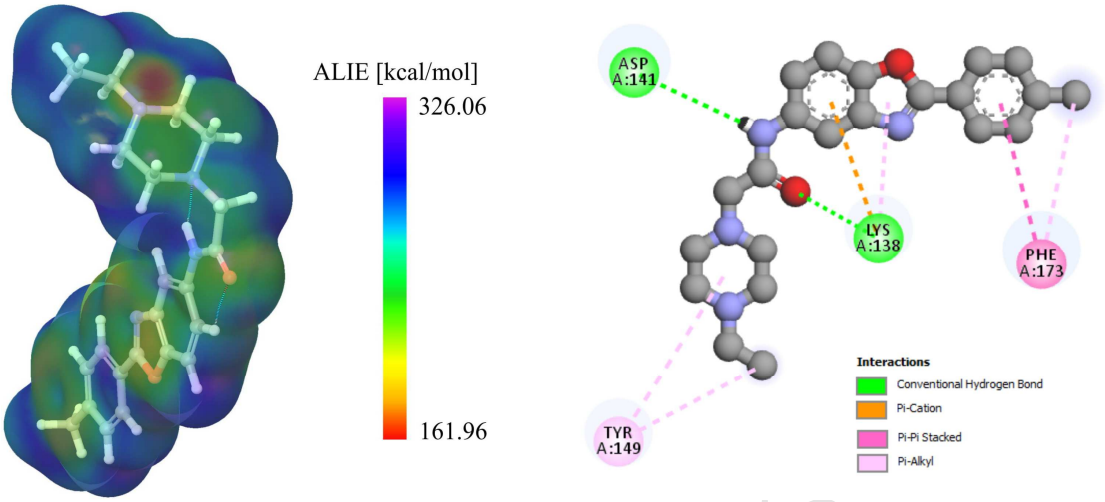

Spectroscopic, antimicrobial and computational study of novel benzoxazole derivative

Shargina Beegum[a], Sheena Mary Y[a], C. Yohannan Panicker[a], Stevan Armaković[b,*], Sanja J. Armaković[c], Mustafa Arisoy[d], Ozlem Temiz-Arpaci[d], Christian Van Alsenoy[e]

[a]Department of Physics, Fatima Mata National College, Kollam, Kerala, India
[b]University of Novi Sad, Faculty of Sciences, Department of Physics, Trg D. Obradovića 4, 21000 Novi Sad, Serbia
[c]University of Novi Sad, Faculty of Sciences, Department of Chemistry, Biochemistry and Environmental Protection, Trg D. Obradovića 3, 21000 Novi Sad, Serbia
[d]Ankara University Faculty of Pharmacy, Department of Pharmaceutical Chemistry, TR-06100, Tandogan, Ankara, Turkey
[e]Department of Chemistry, University of Antwerp, Groenenborgerlaan 171, B-2020, Antwerp, Belgium

*author for correspondence: Stevan Armaković, stevan.armakovic@df.uns.ac.rs

Abstract: A benzoxazole derivative, 2-(*p*-methylphenyl)-5-(2-(4-ethylpiperazine-1-yl)acetamido) benzoxazole (PMPEPAB) has been synthesized and investigated for its spectroscopic properties within the framework of density functional theory (DFT) calculations and molecular dynamics (MD) simulations. Potential energy distribution analysis was employed in order to assign and compare computationally and experimentally obtained wavenumbers. It was identified that the title compound exhibits antibacterial activity against Gram-positive, Gram-negative bacteria and their drug-resistant isolates and a fungus; *Candida albicans.* TD-DFT calculations have been used in order to understand charge transfer within PMPEPAB. Natural bond orbital analysis has been carried out to investigate stability of the molecule arising from charge delocalization and hyper-conjugative interactions. Local reactivity properties have been assessed using the MEP and ALIE surfaces and Fukui functions. Stability in water and sensitivity towards hydrolysis has been investigated by MD simulations and calculations of radial distribution functions, while sensitivity towards autoxidation mechanism has been studied by DFT calculations of bond dissociation energies for hydrogen abstraction. Drug likeness parameters are very competitive, while the binding affinity of the title compound with immunoglobulin tandem protein is –6.4 kcal/mol, indicating that title molecule is a candidate to be active component of a new drug for muscular dystrophy.

Keywords: benzoxazole; DFT; Spectroscopy; ALIE; BDE; RDF.

1. Introduction

Heterocyclic compounds have attracted attention due to their diverse biological and pharmacological properties. Benzoheterocycles such as benzoxazolesare important fragments in medicinal chemistry because of their wide range of biological activities such as antibacterial, antifungal, anti-tubercular, anti-tumoral and antiviral activities [1-8]. In the present study, 2-(*p*-methylphenyl)-5-(2-(4-ethylpiperazine-1-yl)acetamido) benzoxazole (PMPEPAB) was synthesized using a three step procedure and the synthetic pathways for preparation of the target compound with the hope of discovering new effective antimicrobial agent.

Its structure was elucidated with mass and ^{1}H-NMR spectroscopy, while purity was controlled by elemental analysis. In comparison with several control drugs new synthesized benzoxazole derivative has been evaluated for antibacterial and antifungal activity against standard strains and drug-resistant isolates. Beside spectroscopic characterization the aim of this study also encompassed detailed computational investigation of global and local reactive properties.

Global reactive properties of the title molecule have been investigated by visualization of frontier molecular orbitals and calculation of quantum-molecular descriptors such as HOMO-LUMO gap, global hardness and chemical potential. Spectroscopic characterization has been performed by IR, Raman and NMR techniques. DFT approach was also used to theoretically obtain aforementioned spectra, which were then compared with experimentally obtained data. Important local reactivity properties have also been obtained by analysis of molecular electrostatic potential (MEP) and local average ionization energy (ALIE) surfaces.

To evaluate molecule's degradation properties we have considered autoxidation and hydrolysis mechanisms. The motivation for investigation of degradation properties we have found in fact that title molecule could serve as active component of some new pharmaceutics. Taking into account the great stability of pharmaceutical molecules in general it is not strange that natural conditions are not effective enough to decompose them [9], while usual water purification methods are not efficient for their removal [10,11].

Advanced oxidation processes could be very important for the removal of these molecules [10, 12-17]. In these cases DFT calculations and MD simulations [18-21] are used in order to gain an insight into the reactive properties of molecules that need to be degraded. Autoxidation is related to the BDE of hydrogen abstraction and this can be readily performed by DFT

calculations. On the other side important information about molecule's atoms with pronounced interactions with water molecules can be obtained by MD simulations, which also had been performed in this study. Finally, to theoretically confirm the potential of title molecule in terms of biological activity we have performed molecular docking study with the appropriate protein.

2. Experimental details

2.1.Chemistry

The chemicals and solvents were purchased from Sigma-Aldrich Co. (Taufkirchen, Munich Germany) and Fisher Scientific (Pittsburgh, PA, USA) and used without further purification. Silica gel HF_{254}chromatoplates (0.3 mm) were used for TLC and chloroform was employed as mobile phase. Melting points were recorded on a Stuart Scientific SMP 1 (Bibby Scientific Limited, Stone, Staffordshire UK) and are uncorrected. NMR spectra were recorded on a Varian Mercury 400 MHz NMR spectrometer (Palo Alto, CA, USA) in $CDCl_3$; tetramethylsilane (TMS) was used as an internal standard. The mass spectra were recorded on a Waters ZQ Micromass LC-MS spectrometer (Milford, MA, USA) using the ESI(+) method. Elemental analyses were performed on an LECO 932 CHNS (St. Joseph, MI, USA) instrument and results were within ±0.4% of theoretical values. The FT-IR (Fig. 1) and FT-Raman (Fig.2) spectra were recorded using KBr pellets on a DR/Jasco FT-IR 6300 spectrometer and on a Bruker RFS 100/s, Germany.

2.2.General procedure for the preparation of 2-(p-methylphenyl)-5-(2-(4-ethylpiperazine-1-yl)acetamido)benzoxazole

Firstly, 5-Amino-2-(*p*-methylphenyl)-benzoxazole was synthesized by heating 0.02 mol 2,4-diaminophenol·2 HCl (1) with 0.02 mol *p*-methyl benzoic acid in 25 g polyphosphoric acid (PPA) and stirring for about 2 h at 160-180ºC. At the end of the reaction period, the residue was poured over ice and the solution was neutralized with 10% NaOH solution. The resulting precipitate was filtered, washed with distilled water, dissolved in boiling ethanol with 0.2 g charcoal, and filtered off. Crystallization was fulfilled by dissolving the precipitate in ethanol and adding distilled water. The crude compound was obtained by filtration and drying the filtrate under ambient conditions [7]. Secondly, 2-chloroacetyl chloride (0.02 mol) was added over a

period of 1 h to a stirred, ice-cooled mixture of 5-amino-2-(*p*-methylphenyl)-benzoxazole (0.02 mol), sodium bicarbonate (0.02 mol), diethyl ether (40 ml), and water (20 ml). The mixture was stirred overnight. The precipitate formed was filtered off, washed with water and dissolved in ethanol. Crystallization was done by adding distilled water and the crude product was obtained drying the filtrate under ambient conditions [3]. Then 0.002 mol 5-(2-chloroacetamido)-2-(*p*-methylphenyl)-benzoxazole was added to 0.002 mol*N*-ethylpiperazine and 2 ml of triethylamine solution in 3 ml of *N*,*N*-dimethylformamide (DMF) and 2 ml of ethanol.

The mixture was stirred at room temperature for 24 h. At the end of the reaction time, mixture was poured over ice, equal volume of 5% NaOH solution was added and extraction was performed by chloroform. Solvent was evaporated under diminished pressure and resulting crude product was purified by column chromatography using chloroform as mobile phase. Finally, fractions of chloroform were collected, solvent was evaporated and crystallization was fulfilled by dissolving the residue in chloroform and adding petroleum ether.

Crystalline material was dried *in vacuo*. The structure of the compound was supported by spectral data. The ^{1}H-NMR and mass spectra and elemental analysis results agree with those of the proposed structure (atom numbering as indicated in Figure 1). Yield (%): 83; M.P., 156-157°C; Mass m/e (%) 379(100, M+H); Mol. Formula; $C_{22}H_{26}N_4O_2$; Cal./Found: C : 66.04, H: 7.15, N: 14.00, C:65.96, H: 7.01, N: 13.94.^{1}H-NMR (δppm, *J*= Hz):(CDCl3): 1.100-1.137 (3H, t), 2.442-2.705 (13H, m), 3.184 (2H, s), 7.320-7.340 (2H, d, Jo=8.0), 7.497-7.519 (1H, d, Jo=8.8), 7.543-7.569 (1H, dd, Jo=8.4, Jm=2.0), 7.985-7.989 (1H, d, Jm=1.6), 8.119-8.140 (2H, d, Jo=8.4), 9.291 (1H, s).

3. Computational details

DFT theoretical calculations of the title compound was carried out with the Gaussian09 software package [22] using B3LYP/6-311++G(d,p) (5D, 7F) basis set to predict the molecular structure, wavenumbers, natural bond orbital calculations, MEP and frontier molecular orbitals. A scaling factor of 0.9613 was used to scale the theoretically predicted wavenumbers for getting a considerably better agreement with the observed experimental data [23], while the wavenumbers were assigned with the help of potential energy distribution [24] and Gaussview program [25].

Computational study of PMPEPAB has been also done by Schrödinger Materials Science Suite 2016-4. Namely, for DFT calculations and MD simulations, respectively, Jaguar 9.4 [26] and Desmond [27-30] programs were also used in this study. In Jaguar program B3LYP exchange-correlation functional [31] has been also employed together with 6-311++G(d,p), 6-31+G(d,p) and 6-311G(d,p) basis sets for the calculations of ALIE, Fukui functions and BDEs, respectively. Time dependent DFT (TD-DFT) calculations have been performed by full linear response method using CAM-B3LYP [32] exchange-correlation functional and 6-31+G(d,p) basis set. Charge transfer analysis has been done with Multiwfn program [33-36]. Electron density variation and $C_{+/-}$ functions have been visualized with VMD program [37-43], while Tachyon [44] ray tracing library, as implemented in VMD, was used for rendering of figures.

OPLS 3 force field [27, 45-47] was used for MD simulations with Desmond program. Simulation time was set to 10 ns, while temperature was set to 300 K. Also, pressure was set to 1.0325 bar, while cut off radius was set to 12 Å. System was of isothermal–isobaric (NPT) ensemble class. For the solvent a simple point charge (SPC) model [48] was used. MD simulation was done by placing of one PMPEPAB molecule into the cubic box with ~3000 water molecules. Electron density analysis developed by Johnson et al. [49, 50] and implemented in Jaguar program was used for the determination of noncovalent interactions. Maestro GUI [51] was used for the preparation of input files and analysis of results when Schrödinger Materials Science Suite 2016-4 was used.

4. Results and discussion

4.1.Antimicrobial Activity and Microbiological Assays

Materials used in the microbiology study were; Mueller Hinton agar (MHA) (Merck, Darmstadt, Hesse, Germany), Mueller Hinton broth (MHB) (Merck), Sabouraud dextrose agar (SDA) (Merck), RPMI-1640 medium with L-glutamine (Sigma-Aldrich), 3-[*N*-morpholino]-propane-sulfonic acid (MOPS) (Sigma-Aldrich), 96-well micro plates (BD, Franklin Lakes, NJ, USA), transfer pipette (Eppendorf, Hamburg, Germany), ampicillin (Mustafa Nevzat Pharmaceuticals, Istanbul, Turkey), gentamicin sulfate (Paninkret Chem.-Pharm., Pinneberg, Germany), ofloxacin (Zhejiang Huangyan East Asia Chemical CO. Ltd., Huangyan, Zhejiang, China), vancomycin (MaynePharma, Salisbury South, SA, Australia), fluconazole (Sigma-Aldrich), amphotericin B trihydrate (Riedel de Haen, Seelze, Germany), DMSO (Riedel de

Haen). Microorganisms used in the assay were; *Escherichia coli* isolate (has extended spectrum beta lactamase (ESBL) enzyme), *Enterococcus Faecalis*isolate (resistant to vancomycin (VRE)], *Pseudomonas aeruginosa* isolate (resistant to gentamicin), and *Staphylococcus aureus* isolate (resistant to methicilline (MRSA)), *E. coli* ATCC 25922, *E. faecalis* ATCC 29212, *P. aeruginosa* ATCC 25853, *S. aureus* ATCC 29213, *Candida albicans* ATCC 10231.

Clinical isolates and reference strains were provided from Gazi University Hospital Microbiology Laboratory (Ankara, Turkey) and Gazi University Faculty of Pharmacy Department of Pharmaceutical Microbiology Culture Collection (Ankara, Turkey), respectively. Stock solutions of the test compounds were prepared in DMSO. Bacterial susceptibility testing was performed according to the guidelines of CLSI M100-S18 [52]. MHB was added to each well of the micro plates. The bacterial suspensions used for inoculation were prepared at 10^6 CFU/ml by diluting fresh cultures at McFarland 0.5 density. Suspensions of the bacteria at 10^6 CFU/ml were inoculated to the two-fold diluted solution of the compounds. A 10-µl bacterium inoculum was added to each well of the micro plates. There were 10^5 CFU/ml bacteria in the wells after inoculations. Micro plates were incubated at 37°C overnight. Fungal susceptibility testing was performed according to the guidelines of CLSI M27-A3 [53]. RPMI-1640 medium with L-glutamine buffered to pH 7 with MOPS was added to each well of the micro plates. The colonies were suspended in sterile saline and the resulting suspension was adjusted to McFarland 0.5 density (10^6 CFU/ml). A working suspension was prepared by appropriate dilution of the stock suspension. 10 µl of this suspension was inoculated to the two-fold diluted solution of the compound resulting in 5×10^2 CFU/ml in the wells. Micro plates were incubated at 35°C for 24-48 hours. After incubation, the lowest concentration of the compounds that completely inhibited macroscopic growth was determined and reported as minimum inhibitory concentration (MIC). All solvents and diluents, pure microorganisms and pure media were used in control wells. All experiments were done in 3 parallel series. The data on the antimicrobial activity of the compound and the control drugs as MIC (µg/ml) values are given in Table 1.

Table 1. *In vitro* antimicrobial activity of PMPEPAB in comparison with the control drugs (MIC values in µg/ml)

-	E.c.	E.c.*	P.a.	P.a.*	S.a.	S.a.*	E.f.	E.f.*	C.a.
PMPEPAB	128	128	128	128	256	256	128	64	128
Ampicillin	2	128	n.d.	n.d.	2	64	2	2	n.d.
Gentamycin	0.5	>512	0.5	>512	0.125	32	4	32	n.d.
Ofloxacin	<0.0625	64	8	64	0.25	0.25	1	4	n.d.
Vancomycin	n.d.	n.d.	n.d.	n.d.	1	1	1	32	n.d.
Fluconazole	n.d.	n.d.	n.d.	n.d.	n.d.	n.d.	n.d.	n.d.	1
Amphothericin B		n.d.	n.d.	n.d.	n.d.	n.d.	n.d.	n.d.	0.25

E.c.: *E. coli* ATCC 25922
E.c.*: *E. coli* isolate(ESBL)
P.a.: *P. aeruginosa* ATCC 27853
P.a.*: *P. aeruginosa* isolate(resistant to gentamicin)
S.a.: *S. aureus* ATCC 29213
S.a.*: *S. aureus* isolate(MRSA)
E.f.: *E. faecalis* ATCC 29212
E.f.*: *E. faecalis* isolate(VRE)
C.a.: *C. albicans* ATCC 10231
n.d.: Not determined (Microbiological assays were not performed due to following reasons; *P.aeruginosa* is naturally resistant to ampicillin; Gram-negative bacteria employed in the study are naturally resistant to vancomycin; antibacterial drugs were not assayed against fungi; antifungal drugs were not assayed against bacteria)

According to the results presented in Table 1, PMPEPAB compound exhibited significant potential for practical applications in pharmacology. Although antimicrobial activity PMPEPAB is lower in comparison with some known antibiotics, PMPEPAB exhibited broad antibacterial activity with MIC values in the range of 64–256 µg/ml. Although ampicillin is characterized by significantly lower MIC values against several bacteria mentioned in Table 1, it is ineffective in case of the *P. aeruginosa*, for which PMPEPAB exhibited activity characterized by the MIC value of 128 µg/ml. In comparison with gentamycin, PMPEPAB exhibits much better activity against *E. coli* isolate and *P. aeruginosa* isolate. Also according to the Table 1, ofloxacin has better MIC values in comparison with PMPEPAB. However, ofloxacin is ineffective against *C. albicans*, while PMPEPAB has activity against *C. albicans* characterized by the MIC value of 128 µg/ml. Similar conclusions can be drawn when antimicrobial activity of PMPEPAB is compared with vancomycin, fluconazole and amphothericin B, which are ineffective in many cases for which PMPEPAB exhibits activity.

4.2.Geometrical parameters

In order to thoroughly understand molecular structure of the PMPEPAB molecule, its geometrical parameters have been summarized in this chapter. Experimentally and computationally obtained geometrical parameters of PMPEPAB molecule have been also compared in this chapter, in order to validate the employed level of theory. In the following discussion, the rings, N_{37}-C_{38}-C_{39}-N_{34}-C_{35}-C_{36}, C_{12}-C_{13}-C_{15}-C_{18}-C_{16}-C_{14}, C_{12}-C_{13}-N_{22}-C_{11}-O_{21} and C_1-C_2-C_4-C_8-C_6-C_3 have been designated as PhI, PhII, PhIV and PhIII, respectively. Molecular structure of the optimized PMPEPAB molecule has been presented in Figure 1, while geometrical parameters have been summarized in Table S1 of the Supplementary Materials. The numeration of atoms used in Figure 1 has been also used later, in chapter dealing with NMR parameters.

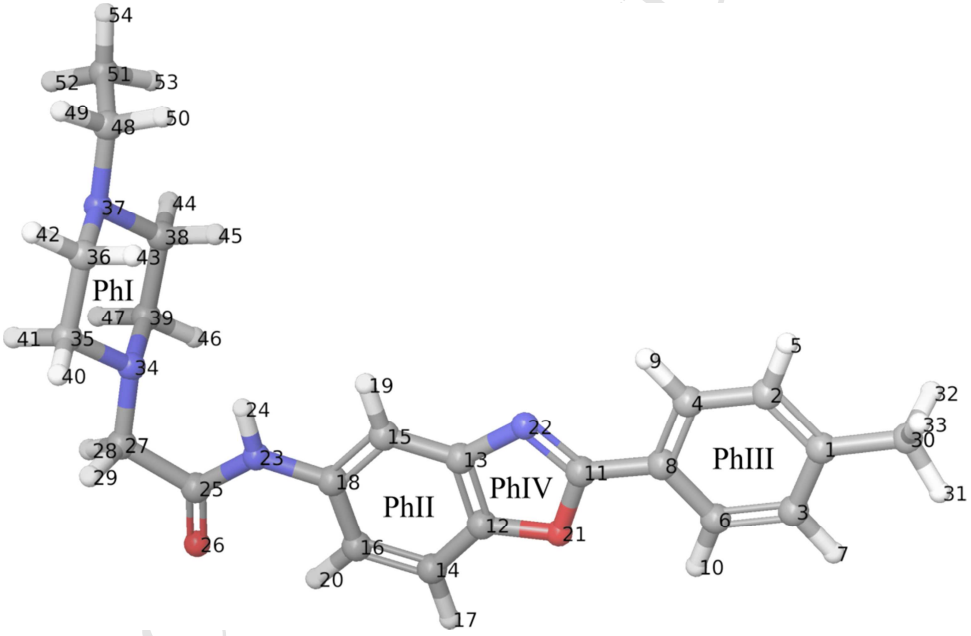

Figure 1. Optimized geometry of PMPEPAB

For the title compound, the C-C bond lengths of the phenyl rings are 1.4126-1.3816 Å, for PhII and 1.4034-1.3868 Å for PhIII, which is in agreement with the reported literature [54]. The C=O bond length of the title compound 1.2204 Å , while the reported value are 1.2188 Å [55]. In the present case, the C-O bond lengths are 1.3783 Å and 1.3731 Å for C_{11}-O_{21} and C_{12}-O_{21}, respectively, and are in agreement with the reported values for a similar derivative (1.3871 Å and 1.3653 Å) [56]. The following bond lengths: C_{11}=N_{22} = 1.2986 Å, C_{13}-N_{22} = 1.3907 Å, C_{18}-N_{23}

=1.4109 Å, C_{25}-N_{23} = 1.3652, C_{27}-N_{34} = 1.4594 and C_{48}-N_{37} = 1.4648 Å differ due to the different environment in the molecular system, while C_{11}-N_{22} has a double bond character as reported in literature [56]. For the piperazine ring of the title compound, the bond lengths are, N_{37}-C_{38} = 1.4614 Å, N_{37}-C_{36} = 1.4612 Å, C_{36}-C_{35} = 1.5249 Å, N_{34}-C_{39} = 1.4687 Å, N_{34}-C_{35} = 1.4667 Å, C_{38}-C_{39} = 1.5248 Å with corresponding reported bond lengths being 1.465, 1.463, 1.514, 1.458, 1.471, 1.511 Å in [57] and 1.4488, 1.485, 1.535, 1.488, 1.477, 1.547 Å in [58]. The DFT calculations provide the following bond angles within the piperazine ring N_{37}-C_{36}-C_{35} = 110.9°, N_{37}-C_{38}-C_{39} = 110.8°, N_{34}-C_{39}-C_{38} = 110.8°, N_{34}-C_{35}-C_{36} = 110.4°, C_{39}-N_{34}-C_{35} = 110.3° whereas the corresponding reported values are 110.0, 109.7, 109.7, 110.0, 110.0° [57]. The dihedral angles of the piperazine ring, C_{38}-N_{37}-C_{36}-C_{35} = -57.8°, C_{39}-N_{34}-C_{35}-C_{36} = -56.9°, N_{37}-C_{36}-C_{35}-N_{34} = 57.8°, C_{35}-N_{34}-C_{39}-C_{38} = 56.7°, C_{36}-N_{37}-C_{38}-C_{39} = 57.3°, N_{34}-C_{39}-C_{38}-N_{37} = -57.2° are in agreement with the reported values in [59]. The interactions between the CH_2 groups and the piperazine ring PhI are evident from the bond angles at N_{37} (C_{36}-N_{37}-C_{38} = 110.1°, C_{36}-N_{37}-C_{48} = 111.8° and C_{38}-N_{37}-C_{48} = 113.3°) and N_{34} (C_{35}-N_{34}-C_{39} = 110.3°, C_{35}-N_{34}-C_{27} = 113.4° and C_{39}-N_{34}-C_{27} =112.2°). At C_{25} position the bond angles are, C_{27}-C_{25}-N_{23} = 113.1°, C_{27}-C_{25}-O_{26} = 120.7° and N_{23}-C_{25}-O_{26} = 126.1° and this asymmetry in angles reveals interaction between the carbonyl group and neighboring CH_2 group at C_{27} position. The interaction between NH and PhII is evident from the bond angles around C_{18} which are C_{15}-C_{18}-C_{16} = 121.0°, C_{15}-C_{18}-N_{23} = 117.0° and C_{16}-C_{18}-N_{23} = 122.1°. Also, around C_{11} position, the bond angle of N_{22}-C_{11}-C_8 is increased by 7.8°, N_{22}-C_{11}-O_{21} is decreased by 5.3° , while C_8-C_{11}-O_{21} is decreased by 2.6° from 120°, which is a consequence of interaction between the PhIV and PhIII rings.

4.3.IR and Raman spectra

The FT-IR and FT-Raman spectra are provided in Figures 2 and 3, respectively, whileTable S2 of the Supplementary Materials contains the calculated and scaled wavenumbers, observed IR and Raman bands and vibrational assignments of the title compound.

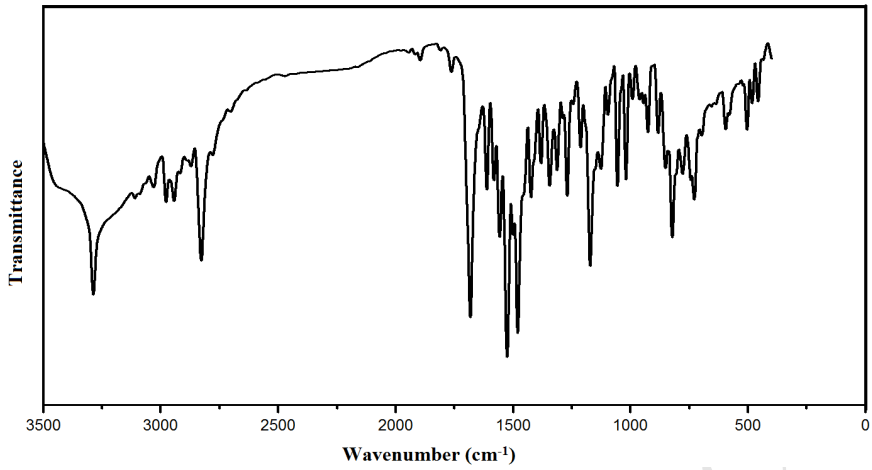

Figure 2. FT-IR spectrum of PMPEPAB

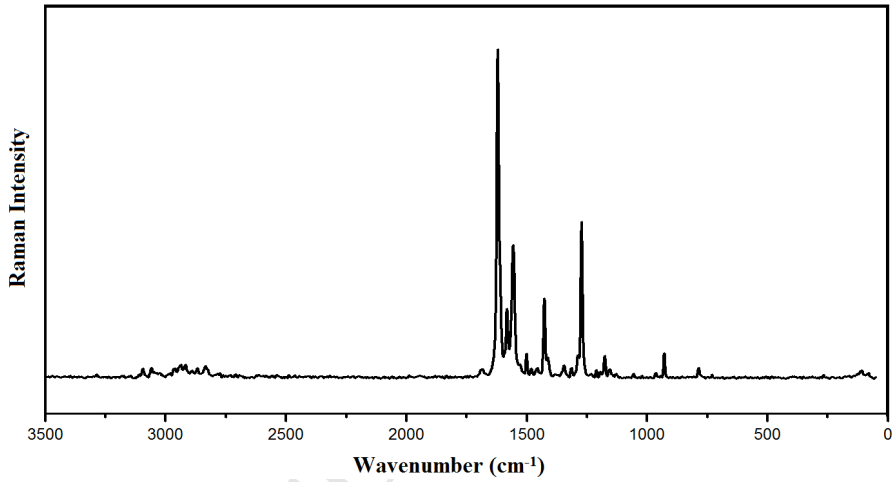

Figure 3. FT-Raman spectrum of PMPEPAB

According to literature [60, 61], the N-H modes are expected in the following ranges: stretching mode: 3500-3300 cm^{-1}; deformation modes: around 1500, 1250 and 750-600 cm^{-1}. For the title compound, the N-H stretching modes are assigned at 3283 cm^{-1} (IR), 3371 cm^{-1} (Raman) and at 3367 cm^{-1} theoretically and the N-H bending modes are assigned in the range 1511-616 cm^{-1} theoretically and experimentally bands are observed at 1507, 1190, 619 cm^{-1} (Raman) and 1508, 1188 cm^{-1} (IR) which are in agreement with literature [55,62].

The C=N stretching mode of the title compound is assigned at 1526 cm^{-1} experimentally and at 1526 cm^{-1} theoretically as expected [63, 64]. The C-N stretching modes of the title compound are assigned in the range 1256-1004 cm^{-1} theoretically [64]. In the present case, the C=O stretching mode is observed at 1680 cm^{-1} experimentally, 1678 cm^{-1} theoretically while the C-O stretching modes are assigned at 1168 cm^{-1} in the IR and at 1167, 1029 cm^{-1} theoretically 64,66].

Mary et al. reported the C=O stretching mode at 1677 cm^{-1} (IR) 1670 cm^{-1} (Raman) and at 1674 cm^{-1} (DFT) [55] and the C-O-C stretching modes in the range 1135-984 cm^{-1} theoretically [67].

The methyl stretching vibrations of the title compound are observed at 2980, 2917, 2895 cm^{-1} (IR) and at 2987, 2980, 2916, 2899 cm^{-1} (Raman) [60,63]. The bending modes of the methyl groups are observed at 1058, 990 cm^{-1} (IR), at 1347, 1054 cm^{-1} (Raman). The DFT calculations give these modes in the ranges of 2984-2906 cm^{-1} (stretching) and 1458-965 cm^{-1} (deformation modes) [60,63].

The CH_2 modes of the title compound are observed at 2873, 2779 cm^{-1} (stretching), 1420, 1246, 1219, 778 cm^{-1} (deformation) in the IR spectrum, 2870, 2782 cm^{-1} (stretching), 1270, 1220 cm^{-1} (deformation) in the Raman spectrum experimentally and the PED analysis gives these modes in the range 2928-2780 cm^{-1} (stretching) and 1458-779 cm^{-1} (deformation modes), which is in agreement with the literature [60, 63].

The phenyl CH stretching modes are assigned at 3112, 3062 cm^{-1} (IR), 3110, 3060 cm^{-1} (Raman), 3114-3059 cm^{-1} (DFT) for PhII and at 3080, 3037 cm^{-1} (IR), 3085, 3040, 3030 cm^{-1} (Raman), 3077-3039 cm^{-1} (DFY) for PhIII [63]. The phenyl ring C-C stretching modes are assigned theoretically in the ranges of 1598-1318 cm^{-1} for PhII and 1588-1284 cm^{-1} for PhIII, while experimentally bands are in the ranges 1608-1282 cm^{-1} (IR) and 1610-1282 cm^{-1} (Raman) [63]. For the title compound the ring breathing mode is assigned at 1100 cm^{-1} theoretically for tri-substituted phenyl ring and at 771 cm^{-1} for para-substituted phenyl ring [68] which are in agreement with the reported values [55, 69-71]. The in-plane CH bending modes of the phenyl rings are assigned at 1130 cm^{-1} (Raman), in the range 1261-1100 cm^{-1} (DFT) for PhII and 1152, 1095, 1017 cm^{-1} (IR), 1291, 1154, 1021 cm^{-1} (Raman), in the range 1290-1019 cm^{-1} (DFT) for PhIII as expected [63]. The out-of-plane CH bending modes of the phenyl rings are assigned at 804 cm^{-1} (IR), 928, 832, 806 cm^{-1} (Raman), in the range 932-804 cm^{-1} (DFT) for PhII and 940 cm^{-1} (IR), 940 cm^{-1} (Raman), in the range 955-810 cm^{-1} (DFT) for PhIII [63].

For the title compound, the CH_2 stretching modes in the piperazine ring are observed at 2944, 2827 cm^{-1} (IR), 2963, 2938, 2834, 2822 cm^{-1} (Raman) and in the range 2965-2795 cm^{-1} theoretically which are in agreement with reported values [72, 73]. For the title compound, the CH_2 deformation modes associated with the piperazine ring are assigned in the ranges, 1450-1058 cm^{-1} (IR), 1453-1036 cm^{-1} (Raman) and in the range 1450-833 cm^{-1} (DFT). According to Spell [74] the CH_2 deformation modes associated with the piperazine ring was found to be

associated with sharp, well defined absorptions at 1380-1345 cm^{-1}, 125-1170 cm^{-1} and 1050-1025 cm^{-1} regions of IR spectrum. In accordance with the findings of Spell [74], we observed a very strong peak in the IR spectrum at 1340 cm^{-1} corresponding to CH_2 wagging mode of the piperazine ring. The theoretically calculated corresponding wave number for this mode is at 1336 cm^{-1}. A very sharp and intense band was observed at 1068 cm^{-1} in the IR spectrum of the title compound as reported by da Silva et al. [75] and was assigned to the ring CH_2 rocking vibration. According to Spell [74], this is one of the most useful bands for detecting the presence of di-substituted piperazines. Piperazine ring stretching modes of the title compound are assigned at 1115, 960, 746 cm^{-1} (IR), 1175, 1110, 963, 905, 749 cm^{-1} (Raman) and in the range 1171-748 cm^{-1} theoretically [57, 58, 73].

NMR spectra

4.4. NMR spectra

The Gauge-Independent Atomic Orbital (GIAO) ^{1}H and ^{13}C chemical shifts calculation of the title compound (Table 2) has been performed within DFT approach [76, 77].

Table 2. The predicted NMR isotropic chemical shifts (with respect to TMS, all values in ppm)

Atom	σ_{TMS}	σ_{calc}	δ_{calc} (σ_{TMS} - σ_{calc})	Atom	σ_{TMS}	σ_{calc}	δ_{calc} (σ_{TMS} - σ_{calc})
C1	196.85	55.79	141.06	H9	32.77	23.88	8.89
C2	196.85	67.47	129.38	H10	32.77	24.30	8.47
C3	196.85	67.45	129.39	H17	32.77	25.11	7.66
C4	196.85	67.31	129.54	H19	32.77	25.57	7.20
C6	196.85	68.88	127.97	H20	32.77	23.48	9.29
C8	196.85	70.90	125.95	H24	32.77	24.10	8.67
C11	196.85	34.22	162.63	H28	32.77	29.45	3.32
C12	196.85	50.32	146.54	H29	32.77	29.28	3.49
C13	196.85	53.90	142.96	H31	32.77	30.33	2.44
C14	196.85	85.49	111.37	H32	32.77	29.75	3.02
C15	196.85	88.67	108.18	H33	32.77	29.88	2.89
C16	196.85	80.04	116.81	H40	32.77	29.76	3.01
C18	196.85	59.67	137.18	H41	32.77	29.45	3.32
C25	196.85	34.26	162.59	H42	32.77	29.76	3.01
C27	196.85	128.74	68.11	H43	32.77	29.68	3.09
C30	196.85	167.89	28.96	H44	32.77	29.45	3.32
C35	196.85	137.17	59.69	H45	32.77	30.13	2.64
C36	196.85	135.32	61.53	H46	32.77	29.56	3.21
C38	196.85	141.16	55.69	H47	32.77	29.87	2.90
C39	196.85	138.85	58.00	H49	32.77	29.83	2.94

C48	196.85	137.77	59.08	H50	32.77	29.89	2.88
C51	196.85	176.22	20.63	H52	32.77	31.17	1.60
H5	32.77	25.04	7.73	H53	32.77	31.07	1.70
H7	32.77	25.13	7.64	H54	32.77	31.32	1.45

The signal at 162.5902 (theoretical) is assigned to the carbonyl carbon C_{25}. Carbon atoms (C_{48} and C_{27}) of the methylene groups resonate at 59.0772 and 68.1112 ppm. The methyl group carbon atom C51 has a signal at 20.6277 ppm theoretically and while the carbon atom at C30 position has values 28.9587. The carbon atoms in the rings have the following chemical shifts (theoretical ranges): 61.5291-55.6947 for the piperazine ring PhI; 146.5352-108.1805 for the phenyl ring PhII and 141.0599-125.9501 for the phenyl ring PhIII. In the ^{1}H-NMR chemical shift values show three ranges for the rings; the first one is 3.3228-2.6389 (theoretical) ppm due to protons on the CH2 groups of the piperazine ring PhI, the second one is 9.2888-7.2036 (theoretical) ppm due to protons on phenyl ring PhII and the last one is 8.8872-7.6434 (theoretical) ppm due to the protons of phenyl ring PhIII. The proton shifts (theoretical) of CH2 groups are C48 and C27 are 2.9398-2.8818 and 3.4862-3.3164 respectively while that of CH3 at C51 and C30 are 1.6963-1.4485 and 3.0241-2.438 and that of NH proton 8.6662 ppm.

4.5.UV spectra and TD-DFT calculations

To obtain full spectral consideration of the title compound we have also performed TD-DFT calculations in order to simulate UV spectra, Figure 4 and Table 3. Within the framework of TD-DFT calculations the formalism of natural transition orbitals [78] was employed in order to determine orbitals that are principally responsible for the lowest energy transition, Figure 5. Besides, analysis of wavefunction, with the help of Multiwfn program, has been performed in order to determine molecule sites with significant electron density variation as a consequence of the lowest energy excitation, Figure 6. The approach as described in reference [79] and as implemented in Multiwfn program was also used in order to calculate and visualize *C* functions in order to determine the nature of the first excitation. Δr coefficient, as introduced in paper [80] was calculated in order to confirm the nature of the first excitation.

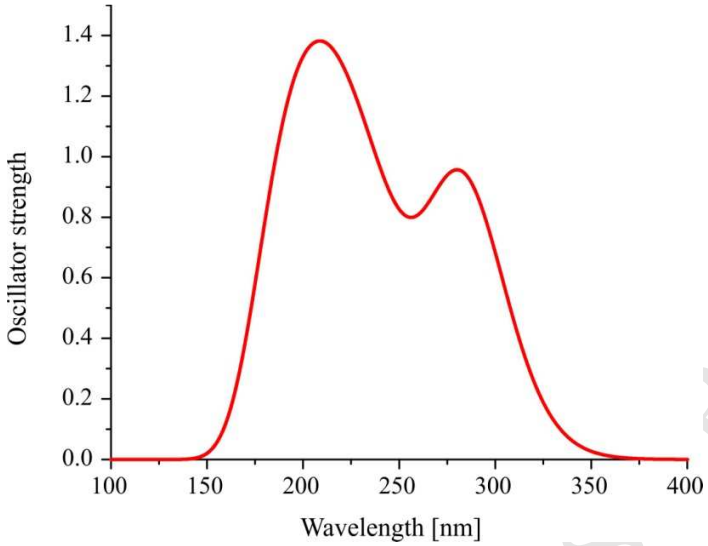

Figure 4. Simulated UV spectra of the PMPEPAB molecule

Table 3. The first 20 excitations of the PMPEPAB compound

Excitation #	Excitation energy [eV]	Wavelength [nm]	Oscillator strength
1	4.34	285.68	0.7954
2	4.89	253.80	0.1998
3	5.00	248.17	0.0375
4	5.44	227.82	0.4847
5	5.51	225.15	0.0108
6	5.61	220.95	0.0930
7	5.98	207.38	0.1132
8	5.99	206.82	0.0238
9	6.02	205.93	0.0015
10	6.06	204.70	0.0003
11	6.08	203.93	0.2470
12	6.11	203.05	0.0017
13	6.25	198.44	0.0010
14	6.29	197.25	0.1473
15	6.31	196.32	0.0142
16	6.34	195.60	0.0103
17	6.43	192.85	0.4215
18	6.49	191.10	0.1786
19	6.52	190.09	0.0269
20	6.66	186.04	0.0088

Simulated UV spectra of PMPEPAB molecule presented in Figure XX1 indicates two distinct absorption peaks located at 280 nm and 208 nm. The first 20 excitations as obtained after TD-DFT calculations have been listed in the Table 3. According to the data summarized in Table

3 it can be seen that the highest oscillator strength (~0.8) has been calculated in the case of the first (the lowest energy) excitation with excitation energy of 4.34 eV located at ~286 nm.

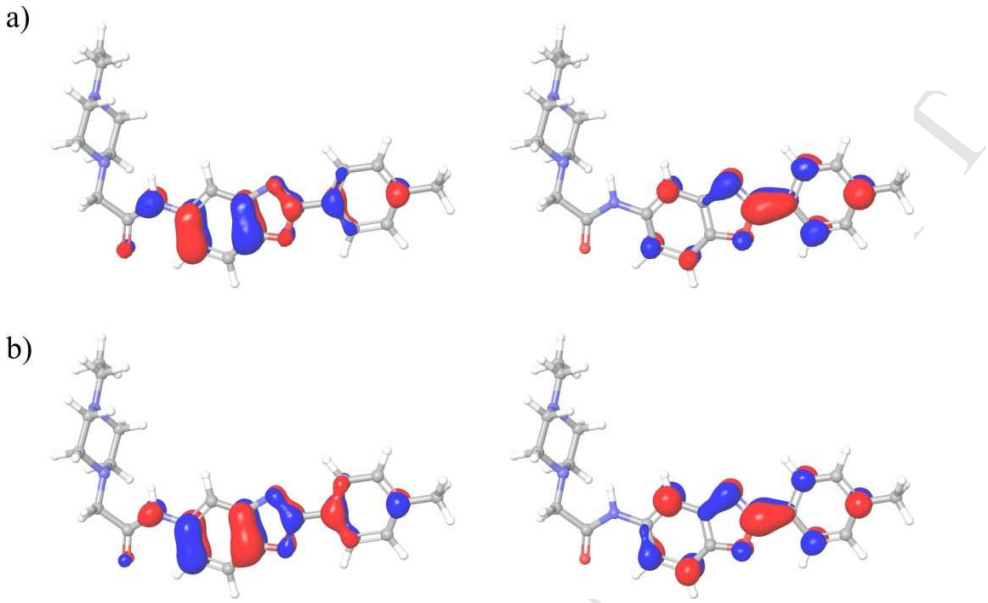

Figure 5. a) HOMO and LUMO orbitals of PMPEPAB and b) hole/particle NTOs of the first excitation of the PMPEPAB molecule

Frontier molecular orbitals as obtained after TD-DFT calculations and hole/particle NTOs of the first excitation provided in Figure 5 clearly match almost perfectly indicating that excitation from HOMO and LUMO orbital principally dictate the lowest energy excitation. The topology of hole and particle NTOs provided in Figure 5 indicate that the highest change in electron density could be expected at three rings within which NTOs have been delocalized. However, in order to more accurately determine which part of the molecule was influenced to highest extent in terms of electron density change we will refer to the electron density variation after the first excitation, Figure 6, which has been obtained by subtracting the electron densities in ground and the first excited state.

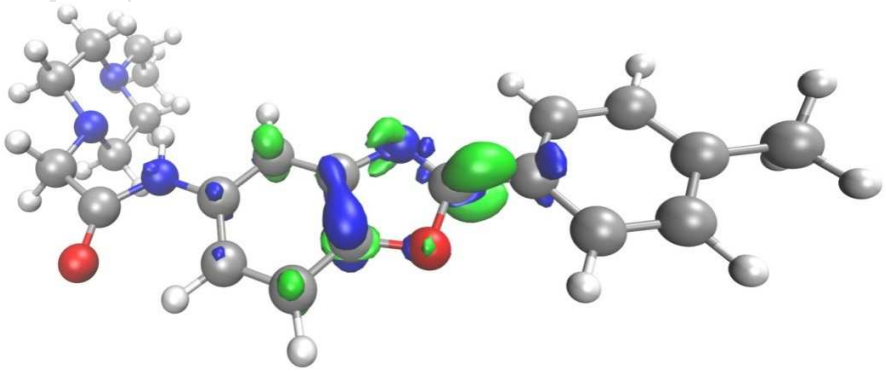

Figure 6. Electron density variation after the first excitation for the PMPEPAB molecule (green and blue colored areas denote positive and negative regions, respectively)

According to location of the electron density variation it can be concluded that the five membered ring is the molecule site with the highest change of electron density. Additionally, electron density variation plot confirms what can be seen at Figure 5, according to which electron excitations occur in the central region of the molecules. Green colored surface in the Figure 6.indicates that electron density increased significantly at carbon atom C11, while it increased significantly at carbon atoms C12 and C13. To clarify the nature of this lowest energy excitation we will further refer to *C* functions, Figure 7, and Δr coefficient.

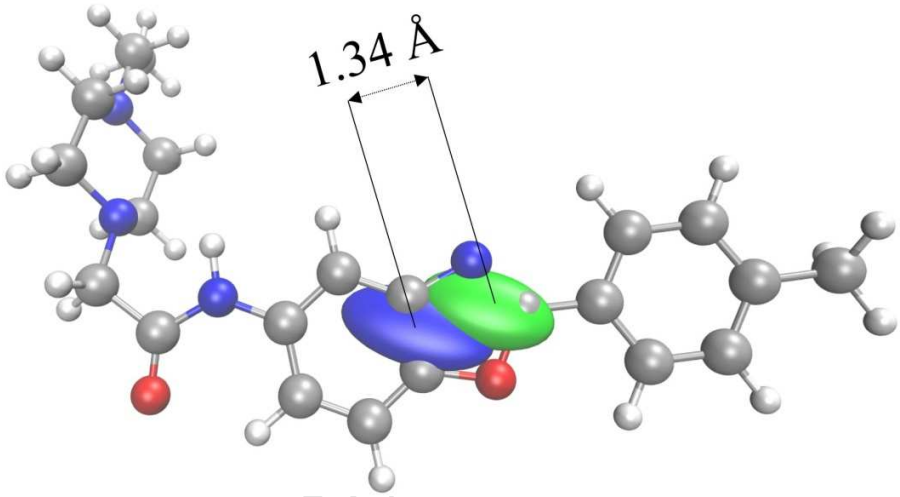

Figure 7.Barycenters of the C_+ and C_- functions of PMPEPAB molecule for the lowest energy excitation

According to the study [79] the distance between barycenters of C_+ and C_- functions is the charge transfer length (CT length), which serves as a measure of the amount of charge transfer. CT length in the case of the lowest energy excitation of PMPEPAB molecule is 1.34 Å, which not high enough value to straightforwardly denote this excitation as charge transfer type. For that reason we have also calculated Δr coefficient, which turned out to have the value of 2.04 Å, a value that determine that the lowest energy excitation is of CT type. Further, thanks to the visualization of barycenters of the C_+ and C_- functions in the case of PMPEPAB it can be also seen that charge transfer occurs from PhII to PhIV ring.

4.6.NBO Analysis

The natural bond orbitals (NBO) calculations were performed using NBO 3.1 program [81] as implemented in the Gaussian09 and the important interactions are given in Tables S3 and S4 of the supplementary materials. The strong interaction $n_1N_{23}\rightarrow\pi^*(C_{25}\text{-}O_{26})$ has the highest E(2) value 61.71 kJ/mol and a very strong interaction has been in $n_2O_{21}\rightarrow\pi^*(C_{11}\text{-}N_{22})$ with an energy of 34.74 kJ/ mol. Almost 100% p-character was observed in π bonding of $C_{11}\text{-}N_{22}$, $C_{12}\text{-}C_{13}$and the lone pairs of O_{21}, N_{23}, O_{26}, N_{34} and N_{37}.

4.7.Frontier molecular orbital analysis

The frontier molecular orbitals are frequently used to initially indicate the interaction of molecule with other species [82-84]. Frontier molecular orbitals, HOMO-LUMO, have been visualized in Fig. 8.

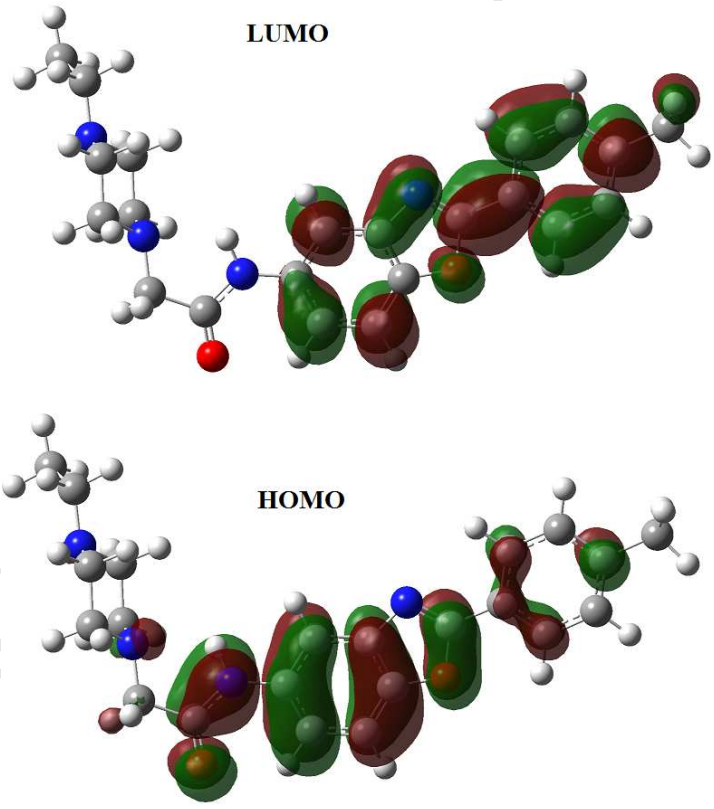

Figure 8. HOMO-LUMO plots of PMPEPAB

It can be seen that HOMO is delocalized over the entire molecule, with the exception of piperazine ring. LUMO on the other side is delocalized over the entire molecule, with the exception of piperazine ring, C=O and NH groups, indicating that the charge transfer occurs within the molecular system. Using the frontier molecular orbital energies, the ionization potential and electron affinity can be determined as: $I = -E_{HOMO}$ and $A = -E_{LUMO}$, respectively. The different chemical descriptors, the hardness (η) and chemical potential (μ) are given by the following relations η = (I-A)/2 and μ = -(I+A)/2. The value of E_{HOMO} = -8.149, E_{LUMO} = -5.226, energy gap = 2.923, global hardness η = 1.462, chemical potential μ = -6.688, global electrophilicity index $\omega = \mu^2/2\eta$ = 15.297 eV in the case of the title compound. The descriptor, molar refractivity (MR) is an important term used in quantitative structure property relationship and is given as, MR = 1.333πNα, where N is the Avogadro number and α is the polarizability of the molecular system [85]. For the title compound, the molar refractivity is 124.08 and this is responsible for the binding property of the molecular system and can be used for the cure of different diseases [86].

4.8.Nonlinear optical properties

Nonlinear optical effect arise from the interactions of electromagnetic fields in various media to produce new fields altered in phase, frequency, amplitude or other propagation characteristics from the incident fields [87]. NLO properties like the dipole moment, polarizability, first and second order hyperpolarizabilities are calculated using B3LYP/6-311++G(d) (5D, 7F). The total molecular dipole moment of the title compound is 3.718 Debye, polarizability is 4.922×10^{-23}e.s.u, and the first and second order hyperpolarizabilities are 4.393×10^{-30} and -46.206×10^{-37}e.s.u. Here, the first hyperpolarizability of the title compound is 33.79 times that of the standard NLO material urea [88] and comparable with the reported values of similar derivatives [56]. The larger component of second order hyperpolarizability is associated with the larger ground state polarization which leads to strong electronic coupling between the ground and the low lying excited state. Also the NLO properties are related to the energy gap between HOMO and LUMO. The energy gap of the title compound is 2.923 eV which is lower than that of urea (6.7 eV) [88]. Therefore, the investigated molecule is suitable for nonlinear optical applications. The potential application of the title compound in the field of nonlinear optics demands the investigation of its structural and bonding features contributing to the hyperpolarizability

enhancement, by analyzing the vibrational modes using the IR and Raman spectrum [89]. The ring stretching bands at 1608, 1581, 1555, 1478, 1403, 1286 cm^{-1} observed in IR spectrum have their counterparts in the Raman spectrum at 1610, 1582, 1555, 1477, 1403, 1282 cm^{-1}, respectively and their intensities in IR and Raman spectra are comparable. The C-N bond lengths in the present case (1.2986-1.4687) are intermediate between those of a C-N single bond (1.48 Å) and a C=N double bond (1.28 Å) and therefore, the calculated data suggest an extended π-electron delocalization of the molecular system which is responsible for the nonlinearity of the title compound [90].

4.9.Molecular Electrostatic Potential

The values of molecular electrostatic potential (MEP) have been mapped to the electron density surface in order to locate sites ofelectrophilic and nucleophilic character [91], Figure 9.

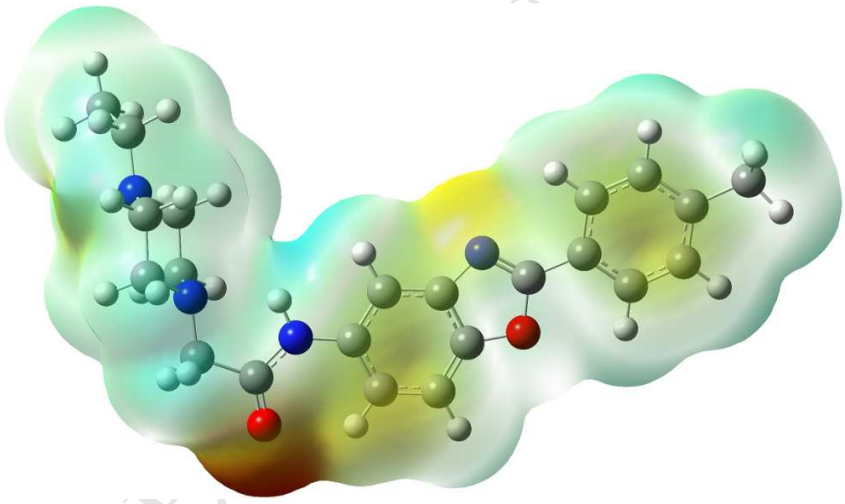

Figure 9. MEP surface of the PMPEPAB molecule

The different values of the electrostatic potential are represented by different colors and potential increases in the order of red < orange < yellow < green < blue. In MEP maximum negative region represents the site for electrophilic attack indicated by red color while the maximum positive region represents nucleophilic attack indicated by blue color. As seen from the MEP map (Fig. 5) of the title compound, regions of negative potential are over the electro negative oxygen atom of the carbonyl group and the regions having the positive potential are over the hydrogen atoms.

4.10. ALIE surface, Fukui functions and noncovalent interactions

ALIE surface has been obtained by mapping of ALIE values to the electron density surface. ALIE is important and frequently employed quantum molecular descriptor which serves as an indicator of molecule sites that are prone to electrophilic attacks. For these purposes it is better than MEP surface, as it directly shows the molecule areas where electrons are least tightly bound. In general, ALIE was defined by Sjoberg et al. [92,93] as a sum of orbital energies weighted by the orbital densities according to the following equation:

$$I(r)=\sum_i \frac{\rho_i(\vec{r})|\varepsilon_i|}{\rho(\vec{r})}, \quad (1)$$

where $\rho_i(\vec{r})$ denotes electronic density of the i-th molecular orbital at the point $\vec{r}$, ε_i denotes orbital energy, while $\rho(\vec{r})$ denotes total electronic density function [94,95]. Representative ALIE surface is provided in Figure 10.

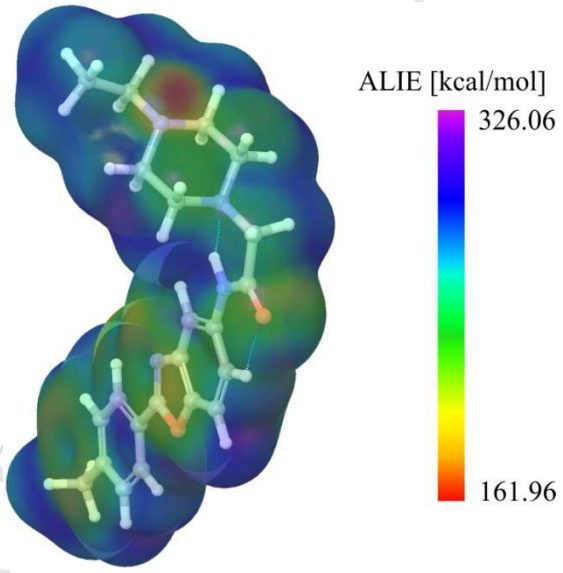

Figure 10. ALIE surface of PMPEPAB molecule

Analysis of Figure 10 indicates that the there is only one molecule site characterized by red color, which indicates the lowest ALIE values. That is molecule area in the near vicinity of nitrogen N37 atom, where ALIE descriptor has values of ~162 kcal/mol. On the other side the highest ALIE values are equal to ~326 kcal/mol and are distributed over the whole molecule in the near vicinities of hydrogen atoms. In Fig.6 intramolecular noncovalent interactions are also presented. It can be seen that within PMPEPAB molecule two noncovalent interactions are

formed, between N34 and H24 and between O26 and H20 atoms, with corresponding strengths of –0.023 and –0.017 electron/bohr^3.

For determination of other reactive sites we have mapped the values of Fukui functions to the electron density surface. By finite difference approach Fukui functions are calculated in Jaguar program according to the following equations:

$$f^{+} = \frac{\left(\rho^{N+\delta}(r) - \rho^{N}(r)\right)}{\delta}, \tag{2}$$

$$f^{-} = \frac{\left(\rho^{N-\delta}(r) - \rho^{N}(r)\right)}{\delta}, \tag{3}$$

where$N$ stands for the number of electrons in reference state of the molecule, while δ stands for the fraction of electron which default value is set to be 0.01 [96]. Representative surfaces of Fukui functions for PMPEPAB molecule have been provided in Figure 11.

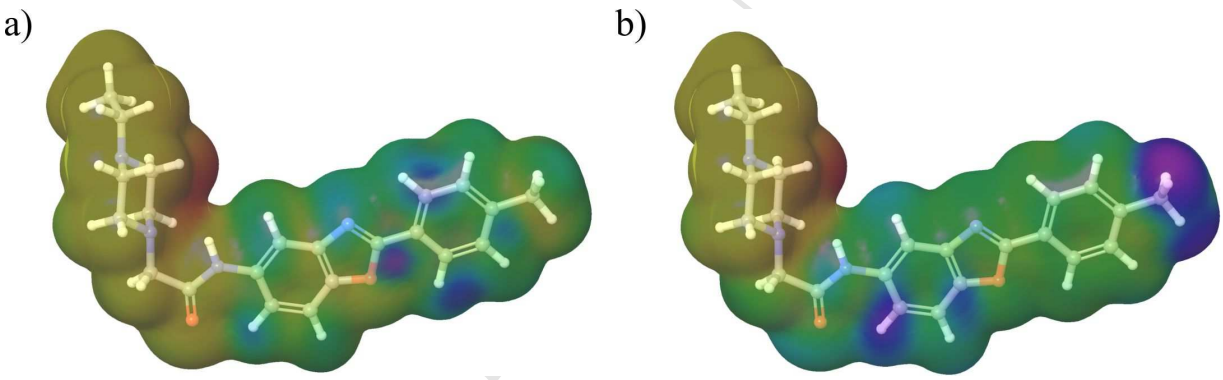

Figure 11.Fukui function a) f^{+} and b) f^{-} of PMPEPAB molecule

In Figure 11, positive (purple) color in Figure 11a shows areas where electron density increased after addition of charge, while negative (red) color in Figure 11b shows areas where electron density decreases after removal of charge. In the case of PMPEPAB molecule in Figure 11a it can be concluded that positive values are located in the near vicinity of benzene ring and oxygen atom of five membered ring, designating these molecule sites as ones where electron density increases as a consequence of addition of charge. Figure 11b indicates that negative values of Fukui f^{-} function are located in the near vicinity of hydrogen atoms belonging to piperazine ring, designating them as locations where electron density decreases as a consequence of charge removal.

4.11. Reactive and degradation properties based on autoxidation and hydrolysis

Computational studies based on DFT calculations and MD simulations offer possibilities to optimize and rationalize various experimental procedures [97-100]. Oxidation reactions are very important degradation pathways of pharmaceutical molecules and organic materials [101-103] and therefore in present study we have assessed the sensitivity of PMPEPAB molecule in the cases of autoxidation and hydrolysis mechanisms. Pharmaceutical molecules are sensitive to autoxidation mechanism only at certain molecule sites. These molecule sites are characterized by BDEs for hydrogen abstraction in the range of 70 to 85 kcal/mol [104,105]. BDE values between 85 and 90 kcal/mol could also be of importance for autoxidation mechanism [105]. BDE values lower than 70 kcal/mol are not favored for autoxidation mechanism [18, 104, 106]. BDE values for all single acyclic bonds in the case of PMPEPAB molecule are presented in Figure 12.

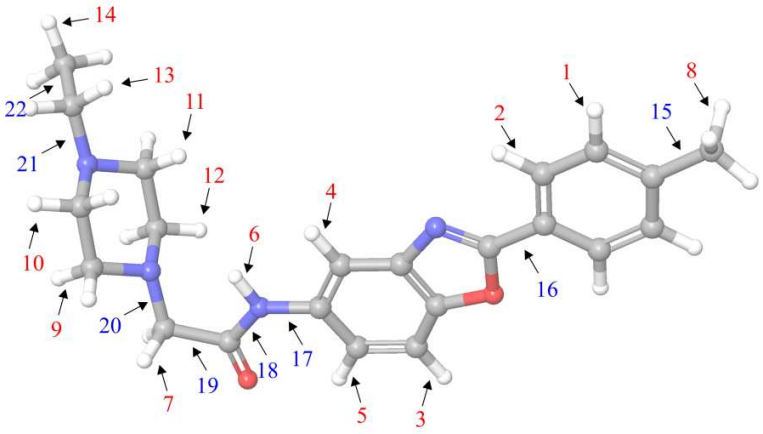

Bond	BDE [kcal/mol]
1	117.05
2	117.68
3	117.89
4	119.48
5	118.19
6	104.69
7	91.09
8	91.21
9	97.91
10	95.89
11	95.72
12	98.09
13	95.74
14	105.29
15	101.69
16	125.02
17	112.33
18	83.74
19	75.80
20	74.21
21	74.99
22	80.10

Figure 12.BDEs of all single acyclic bonds of PMPEPAB molecule

BDE values for hydrogen abstraction indicate that PMPEPAB molecule is stable towards autoxidation mechanism. There are however two values (denoted with numbers 7 and 8 in Figure 12) of BDE that are close to 90 kcal/mol. All other BDE values for hydrogen abstraction are much higher than 90 kcal/mol. This leads to the conclusion that PMPEPAB molecule is stable in the presence of oxygen or in the open air. This is significant for the long-term storage properties of title compound, but it also hardens its degradation in water. The lowest BDE values of the rest

of the single acyclic bonds are denoted with numbers 20 and 21 in Figure 12, indicating that degradation of molecule could start with detaching of piperazine moiety or with the detaching of the terminal ethyl group.

Atoms of PMPEPAB molecule with pronounced interactions with water molecules have been detected by calculation of RDF, g(*r*), which determines the probability of finding a particle in the distance *r* from another particle [107]. The results are presented in Figure 13.

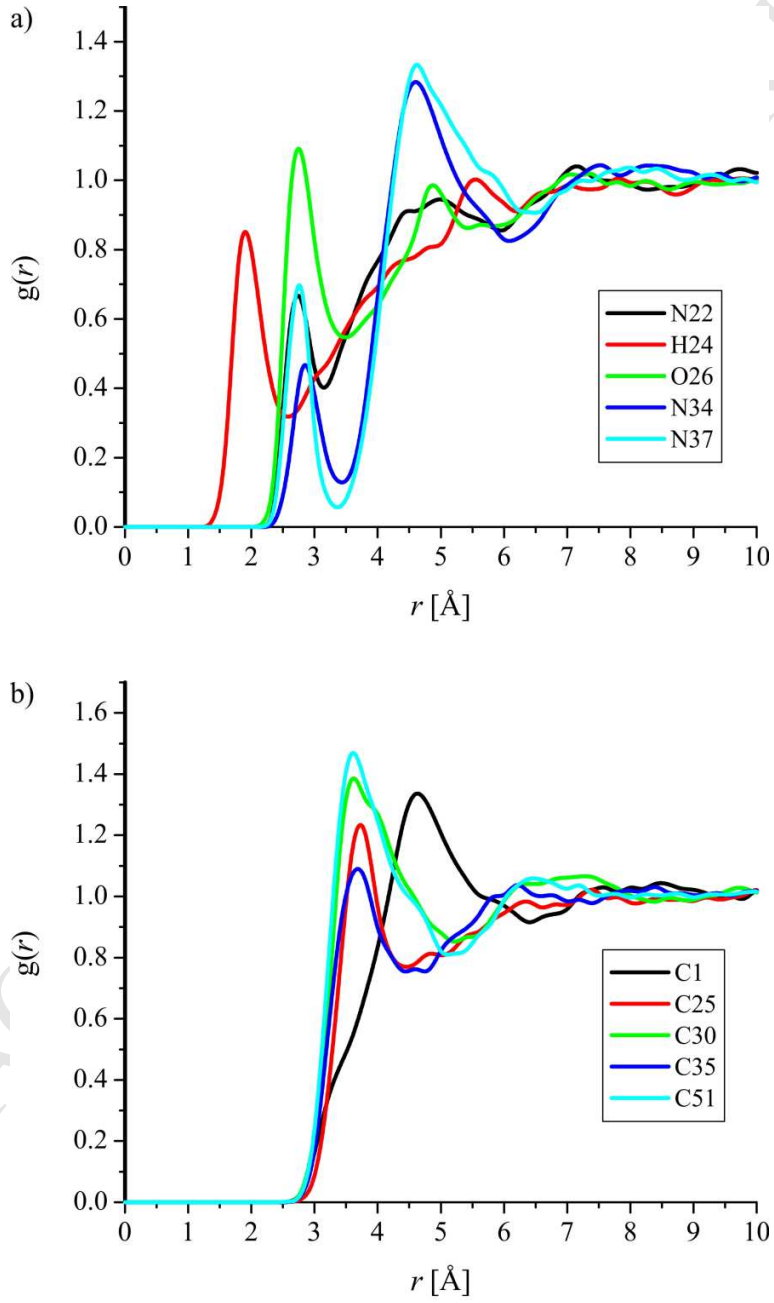

Figure 13.RDFs of atoms of PMPEPAB molecule with significant interactions with water

Results in the case of RDFs in Figure 13, indicate that at least 10 atoms of PMPEPABmolecule have relatively pronounced interactions with water molecules. All but one relevant carbon atoms, Fig.9b, have the maximal g(r) value located at the distance of around 3.6 Å, with maximal g(r) value ranging from 1.1 to almost 1.5. Contrary to them, carbon atom C1 has maximal g(r) value of around 1.3, located at distance of around 4.7 Å. Concerning the non-carbon atoms, Fig.9a, the most pronounced interactions with water exhibits hydrogen atom H24, with maximal g(r) value of around 0.85 located at distance below 2 Å. Nitrogen atoms N34 and N37 are of very similar profiles, characterized with two distinct solvation spheres, with second one having much higher maximal g(r) value. Oxygen atom O26 turned out also to have pronounced interactions with water molecules, characterized by maximal g(r) value of around 1.1 located at distance of around 2.8 Å.

4.12. Drug likeness and molecular Docking

In order to initially assess the potential of PMPEPAB as a prospective drug candidate we have calculated several well established descriptors that are frequently used to evaluate drug likeness of candidates, Table 4.

Table 4. Drug likeness parameters of PMPEPAB molecule

Descriptor	Value
Hydrogen Bond Donor (HBD)[1]	1
Hydrogen Bond Acceptor (HBA)[1]	3
Mass[1]	378
AlogP[1]	3.15
ClogP[2]	3.14
logS[2]	–3.56
Polar surface area (PSA)[1] [Å^2]	61.60
Molar refractivity[1]	108.50
Number of atoms[1]	54
Number of rotatable bonds[1]	5

[1] Calculated with Maestro, [2] Calculated with ALOGPS 2.1. program[108-115]

According to the Lipinski's rule of five [116,117], in order for drug to be orally active in humans a moderately lipophilic character is desired in combination with less than 5 and 10 HBD and HBA, respectively, while mass should be lower than 500 u. Results presented in Table

4indicate that PMPEPAB molecule fulfills all of these prerequisites. Beside aforementioned requirements for screening of drug candidate molecules Ghose et al. [114] proposed that molar refractivity should be in the range of 40–130, number of atoms should be somewhere between 20 and 70, while PSA shouldn't take values above 140 $Å^2$. According to the results presented in this work PMPEPAB molecule clearly fulfills these hardened criteria.

Additionally, according to Veber et al. [118] good oral bioavailability is characterized by number of rotatable bonds lower than 10, which is prerequisite that is also fulfilled by newly synthetized PMPEPAB molecule.

It is also very important to mention that relevant drug likeness descriptors of PMPEPAB molecule have values that are very close to ones that mark some molecule as lead-like compound. Related to efficient lead discovery Congreeveet al. [119] have defined the "rule of three", according to which logP value shouldn't be higher than 3, molecule mass shouldn't be higher than 300 a, while HBD, HBA and number of rotatable bonds shouldn't be higher than 3. Results presented in Table S1 indicate that PMPEPAB molecule almost meets these harsh requirements. Namely, AlogP [120] in the case of PMPEPAB molecule is just a little bit higher than the desired value of 3, while the number of rotatable bonds exceeds the desired value for 2. Nevertheless, these results indicate that structure of PMPEPAB molecule is close to the structure which would meet all of the harsh prerequisites defined by Congreeve et al. These results also serve as motivation for further studies of similar structures.

Using the Prediction of Activity Spectra (PASS) [121] online tool, possible biological activities of PMPEPAB molecule have been predicted. The PASS program is based on the concept of the biological activity spectrum and uses the structural descriptors in form of multilevel neighborhoods of atoms [121]. PASS program returns results in form of the likelihoods for a certain activity type – Pa and Pi. Pa designates probability of the studied molecule to exhibit certain activity, while Pi designates probability of the studied molecule to be inactive with respect to the certain activity. Results of PASS tool have been summarized in Table 5.

Table 5. Prediction for the activity spectrum of the title compound.

Pa	Pi	Activity
0.671	0.019	Proteasome ATPase inhibitor
0.631	0.018	General pump inhibitor
0.613	0.005	Muscular dystrophy treatment
0.606	0.024	Muramoyltetrapeptidecarboxypeptidase inhibitor
0.567	0.016	Histamine release inhibitor
0.561	0.016	5 Hydroxytryptamine release inhibitor
0.536	0.011	Neuropeptide Y2 antagonist
0.534	0.014	Transcription factor STAT3 inhibitor
0.555	0.040	Gastrin inhibitor
0.526	0.016	Transcription factor STAT inhibitor
0.521	0.013	Mediator release inhibitor
0.516	0.045	Insulysin inhibitor
0.435	0.004	Orexin receptor 1 antagonist
0.425	0.021	Focal adhesion kinase 2 inhibitor
0.373	0.012	Amyloid beta precursor protein antagonist
0.461	0.105	Acute neurologic disorders treatment
0.403	0.052	Neuropeptide Y4 antagonist
0.412	0.063	Polarisation stimulant
0.350	0.004	Orexin receptor antagonist
0.352	0.011	Dual specificity phosphatase inhibitor
0.366	0.032	Transcription factor inhibitor
0.340	0.016	Systemic lupus erythematosus treatment
0.394	0.077	Beta glucuronidase inhibitor
0.443	0.128	Calcium channel (voltage-sensitive) activator
0.355	0.050	Antiamyloidogenic

PASS program indicated the probabilities for certain activities of the PMPEPAB. Since piperazine and its derivatives are known to be useful for treating or preventing neuronal damage, particularly damage associated with neurological diseases, we have decided to specifically pay attention to the possibility that PMPEPAB could be used for the treatment of muscular dystrophy, which is predicted by PASS tool with the Pa value of 0.613.

Muscular dystrophy is a group of disorders characterized by a progressive loss of muscle mass and consequent loss of strength. The most common form of muscular dystrophy is Duchenne muscular dystrophy - typically affects young boys, but other variations can strike in adulthood. Currently, there is no cure for muscular dystrophy, but certain physical and medical treatments can improve symptoms and slow the disease's progression [122]. There is an urgent

need to discover the drug for Muscular dystrophy. Piperazine and its derivatives are especially useful for treating or preventing neuronal damage, particularly damage associated with neurological diseases [123, 124].

All these facts motivated us to study the docking of PMPEPAB molecule against the protein related to muscular dystrophy. For these purposes, high resolution crystal structure of dehydrogenase inhibitor was downloaded from the RSCB protein data bank website with PDB ID: 2J8O. The 2J8O is related to the giant muscle protein called titin, which is characterized by more than 300 predicted titin domains, folded as immunoglobulin or fibronectin modules [125-129]. The majority of identified functions of titin are participated by these domains [129]. 2J8O represents the structure of immunoglobulin domain tandem A168-A169, which is characterized by the specific structural segment responsible for the binding of MuRF-1 ligand.

All molecular docking calculations were performed with Auto Dock-Vina software [130], as reported in literature [54]. The docking protocol predicted the same conformation as was present in the crystal structure with RMSD value well within the reliable range of 2 Å [131]. Amongst the docked conformations, one which binds well at the active site was analyzed for detailed interactions in Discovery Studio Visualizer 4.0 software. The ligand binds at the active site of the substrate by weak non-covalent interactions and these interactions are depicted in Figure 14, while values of binding affinities of several representative docking modes have been summarized in Table 6.

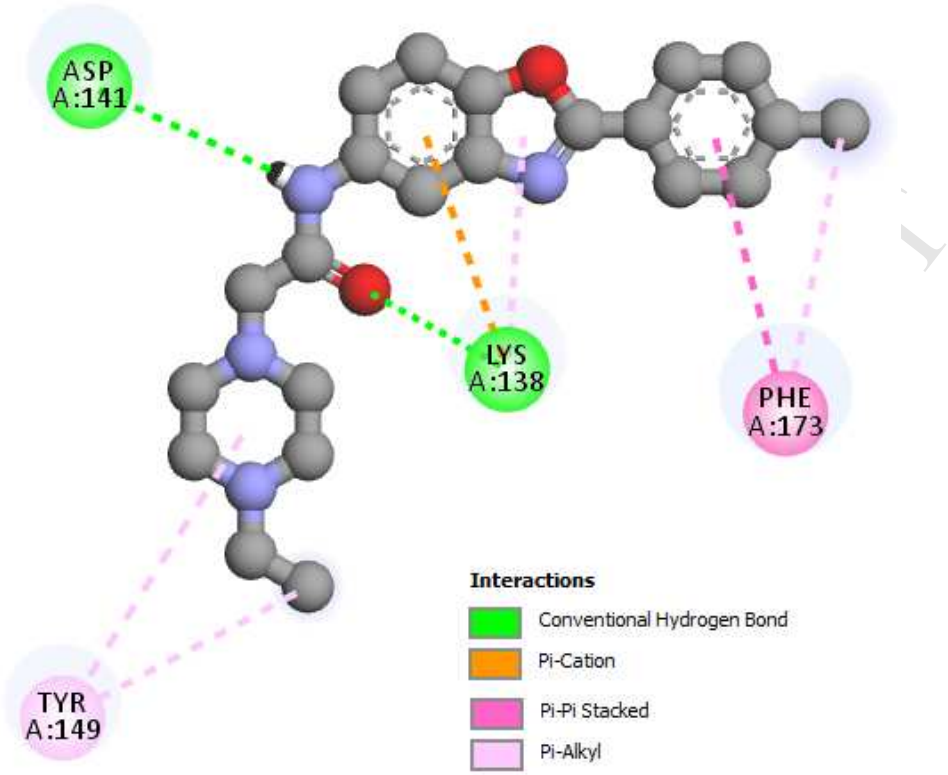

Figure 14.2D diagram of the detailed interaction of ligand with receptor

Table 6. The binding affinity values estimated by the docking study with AutoDock Vina program

Mode	Affinity [kcal/mol]	Distance from best mode[Å]	
		RMSD 1.b*	RMSD u.b**
1	–6.4	0.000	0.000
2	–6.2	2.755	3.232
3	–6.0	17.288	19.672
4	–6.0	19.386	19.970
5	–6.0	19.492	20.136
6	–6.0	7.462	10.992
7	–5.8	1.947	3.183
8	–5.8	18.842	20.671
9	–5.7	5.786	10.217

*RMSD l.b denotes RMSD lower bound, while **RMSD u.b denotes RMSD upper bound

The binding affinity of docked ligand with immunoglobulin tandem protein was estimated to be –6.4 kcal/mol and the complex shown in Figure 15 could be stable. According to these results

the title compound could become a lead compound for developing new drug for muscular dystrophy.

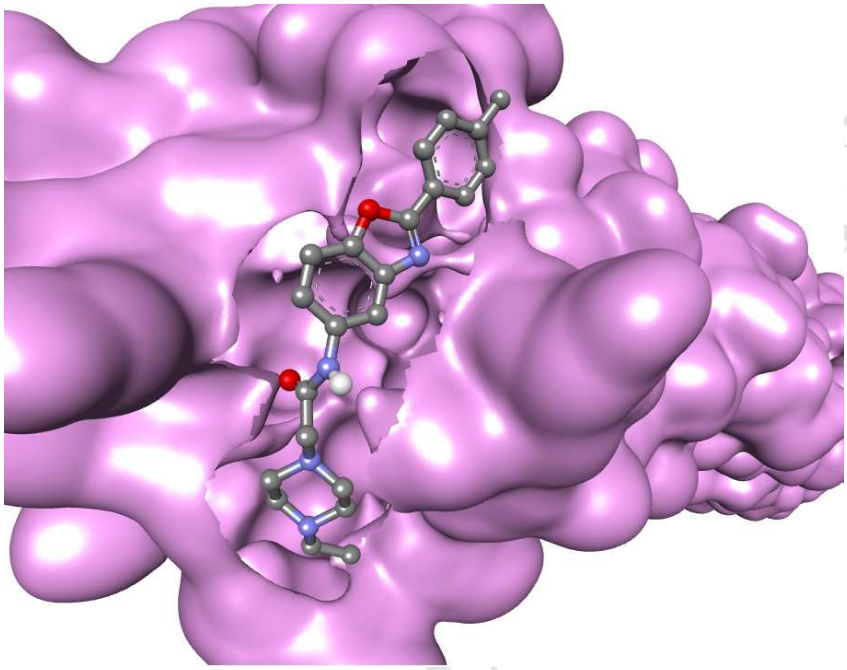

Figure 15.Surface view of ligand at the active site of the receptor

5. Conclusions

The synthesis, vibrational spectral analysis and antimicrobial activity of the title compound are reported. The calculated value of the first hyperpolarizability is almost 34 times higher than in case of the urea molecule, exhibiting the potential of PMPEPAB for NLO applications. The frontier molecular orbital analysis indicates that the lowest excitation is the consequence of the charge transfer from HOMO to LUMO, while the analysis of electron density variation in case of the first excitation indicates that the first excitation is of charge transfer type. MEP and ALIE surfaces have been analyzed in order to understand local reactive properties of PMPEPAB. Particularly, ALIE surface determined that near vicinity of nitrogen atom N34 could be particularly sensitive towards electrophilic attacks. Analysis of electron density between atoms revealed two relatively strong intramolecular noncovalent interactions. Fukui functions also recognized benzene and piperazine rings as possible reactive centers. BDEs for hydrogen abstraction indicate stability towards autoxidation mechanism. RDFs after MD simulations revealed 10 atoms with relatively important interactions with water molecules, among which the

most important is certainly hydrogen atom H24, with maximal g(r) value located at distance below 2 Å. Drug likeness parameters in conjunction with molecular docking results indicate great potential of the title compound for the development of new drug for muscular dystrophy.

Acknowledgment

Part of this study was conducted within the project funded by the Ministry of Education, Science and Technological Development of Serbia, grant III41017.

References

[1] M. Prudhomme, J. Guyot, G. Jeminet, J Antibiot. (Tokyo), 39 (1986) 934-937.
[2] J.P. Haansuu, K.D. Klika, P.P. Söderholm, V.V. Ochaveranko, K. Pihlaja, K.K. Haahtela, P.M. Vuorela, J. Ind. Microbiol. Biotechnol. 27 (2001) 62-66.
[3] M. Arisoy, O. Temız-Arpaci, I. Yıldız, F. Kaynak-Onurdag, E. Akı, I. Yalcın, U. Abbasoglu, Sar.Qsar. Environ. Res. 19 (2008) 589-612.
[4] M. Arisoy, O. Temız-Arpaci, F. Kaynak-Onurdag, S. Ozgen, Z Naturforsch. 68C (2013) 453-460.
[5] M. Arisoy, O. Temız-Arpaci, F. Kaynak-Onurdag, S. Ozgen, Z Naturforsch, 67C (2012) 466-472.
[6] O. Temiz-Arpacı, B.E. Cıfcıoglu-Goztepe, F. Kaynak-Onurdag, S. Ozgen, F.S. Senol, I. Erdogan-Orhan, Acta Biol. Hungarica, 64 (2013) 249-261.
[7] M. Arisoy, O. Temız-Arpaci, F. Kaynak-Onurdag, S. Ozgen, Z Naturforsch, 69C (2014) 368-374.
[8] N. Dawn, D.N. Ward, D.C. Talley, M. Tavag, S. Menji, P. Schaughency, A. Baier, P.J. Smith, Bioorg. Med. Chem. Lett. 24 (2014) 609-612.
[9] S. Armaković, S.J. Armaković, J.P. Šetrajčić, I.J. Šetrajčić, J. Mol. Model. 18 (2012) 4491-4501.
[10] S.J.Armaković, S. Armaković, N.L. Finčur, F. Šibul, D. Vione, J.P. Šetrajčić, B. Abramović, RSC Adv. 5 (2015) 54589-54604.
[11] M.Blessy, R.D. Patel, P.N. Prajapati, Y. Agrawal, J. Pharm. Anal. 4 (2014) 159-165.
[12] B.Abramović, S. Kler, D. Šojić, M. Laušević, T. Radović, D. Vione, J. Hazard.Mater.198 (2011) 123-132.
[13] M.Šćepanović, B.Abramović, A.Golubović, S.Kler, M.Grujić-Brojčin, Z.Dohčević-Mitrović, B.Babić, B.Matović, Z.V. Popović,J. Sol-Gel Sci.Techn. 61 (2012) 390-402.
[14] D.D. Četojević-Simin, S.J. Armaković, D.V. Šojić, B.F. Abramović, Sci. Total Environ. 463 (2013) 968-974.
[15] A. Golubović, B. Abramović, M. Šćepanović, M. Grujić-Brojčin, S. Armaković, I. Veljković, B. Babić, Z. Dohčević-Mitrović, Z.V. Popović, Mater. Res. Bull 48 (2013) 1363-1371.

[16] M. Grujić-Brojčin, S. Armaković, N. Tomić, B. Abramović, A. Golubović, B. Stojadinović, A. Kremenović, B. Babić, Z. Dohčević-Mitrović, M. Šćepanović, Mater.Charact. 88 (2014) 30-41.
[17] S.J. Armaković, M. Grujić-Brojčin, M. Šćepanović, S. Armaković, A. Golubović, B. Babić, B.F. Abramović, Arab. J. Chem. (2017) http://dx.doi.org/10.1016/j.arabjc.2017.01.001.
[18] P. Lienard, J. Gavartin, G. Boccardi, M. Meunier, Pharm. Res. 32 (2015) 300-310.
[19] G.L. de Souza, L.M. de Oliveira, R.G. Vicari, A. Brown, J. Mol. Model. 22 (2016) 1-9.
[20] Z. Sroka, B. Żbikowska, J. Hładyszowski, J. Mol. Model. 21 (2015) 1-11.
[21] H. Djeradi, A. Rahmouni, A. Cheriti, J. Mol. Model. 20 (2014) 1-9.
[22] Gaussian 09, Revision C.01, M.J. Frisch, G.W. Trucks, H.B. Schlegel, G.E. Scuseria, M.A. Robb, J.R. Cheeseman, G. Scalmani, V. Barone, B. Mennucci, G.A. Petersson, H. Nakatsuji, M. Caricato, X. Li, H.P. Hratchian, A.F. Izmaylov, J. Bloino, G. Zheng, J.L. Sonnenberg, M. Hada, M. Ehara, K. Toyota, R. Fukuda, J. Hasegawa, M. Ishida, T. Nakajima, Y. Honda, O. Kitao, H. Nakai, T. Vreven, J.A. Montgomery, Jr., J.E. Peralta, F. Ogliaro, M. Bearpark, J.J. Heyd, E. Brothers, K.N. Kudin, V.N. Staroverov, T. Keith, R. Kobayashi, J. Normand, K. Raghavachari, A. Rendell, J.C. Burant, S.S. Iyengar, J. Tomasi, M. Cossi, N. Rega, J.M. Millam, M. Klene, J.E. Knox, J.B. Cross, V. Bakken, C. Adamo, J. Jaramillo, R. Gomperts, R.E. Stratmann, O. Yazyev, A.J. Austin, R. Cammi, C. Pomelli, J.W. Ochterski, R.L. Martin, K. Morokuma, V.G. Zakrzewski, G.A. Voth, P. Salvador, J.J. Dannenberg, S. Dapprich, A.D. Daniels, O. Farkas, J.B. Foresman, J.V. Ortiz, J. Cioslowski, D.J. Fox, Gaussian, Inc., Wallingford CT, 2010.
[23] J.B. Foresman, in: E. Frisch (Ed.), Exploring Chemistry with Electronic Structure Methods: a Guide to Using Gaussian, Gaussian Inc., Pittsburgh, PA, 1996.
[24] J.M.L. Martin, C. Van Alsenoy, GAR2PED, a Program to Obtain a Potential Energy Distribution form a Gaussian Archive Record, University of Antwerp, Belgium, 2007.
[25] R. Dennington, T.Keith, J. Millam, GaussView, Version 5, Semichem Inc., Shawnee Mission KS, 2009.
[26] A.D. Bochevarov, E. Harder, T.F. Hughes, J.R. Greenwood, D.A. Braden, D.M. Philipp, D. Rinaldo, M.D. Halls, J. Zhang, R.A. Friesner, Int. J. Quantum Chem. 113 (2013) 2110-2142.
[27] D. Shivakumar, J. Williams, Y. Wu, W. Damm, J. Shelley, W. Sherman, J. Chem. Theory Comput. 6 (2010) 1509-1519.
[28] Z. Guo, U. Mohanty, J. Noehre, T.K. Sawyer, W. Sherman, G. Krilov, Chem. Biol. Drug Design, 75 (2010) 348-359.
[29] K.J. Bowers, K.J., E. Chow, H. Xu, R.O. Dror, M.P. Eastwood, B.A. Gregersen, J.L. Klepeis, I. Kolossvary, M.A. Moraes, F.D. Sacerdoti. Scalable algorithms for molecular dynamics simulations on commodity clusters.in*SC 2006 Conference, Proceedings of the ACM/IEEE*. 2006. IEEE.
[30] V.B. Bregović, N. Basarić, K. Mlinarić-Majerski, Coord. Chem. Rev. 295 (2015) 80-124.
[31] A.D. Becke, J. Chem. Phys. 98 (1993) 5648-5652.
[32] T.Yanai, D.P. Tew, N.C. Handy, Chem. Phys.Lett. 393 (2004) 51-57.
[33] T.Lu, F. Chen, J.Comput.Chem. 33 (2012) 580-592.
[34] T.Lu, F. Chen, J. Mol. Graph. Model. 38 (2012) 314-323.
[35] L. Tian, C. Feiwu, *Calculation of molecular orbital composition.* (2011).
[36] M. Xiao, T. Lu, J. Adv.Phys. Chem. 4 (2015) 111-124.

[37] W. Humphrey, A. Dalke, K. Schulten, J. Mol.Graph. 14 (1996) 33-38.

[38] J.E. Stone, J. Gullingsrud, K. Schulten. *A system for interactive molecular dynamics simulation*. in *Proceedings of the 2001 symposium on Interactive 3D graphics*. 2001. ACM.

[39] J. Eargle, D. Wright, Z. Luthey-Schulten, Bioinformatics 22 (2006) 504-506.

[40] D.Frishman, P. Argos, Proteins 23 (1995) 566-579.

[41] A. Varshney, J. Frederick P. Brooks, W.V. Wright, *Linearly Scalable Computation of Smooth Molecular Surfaces*, IEEE CG&A 1994.

[42] M.F. Sanner, A.J. Olson, J.-C. Spehner. *Fast and robust computation of molecular surfaces*,Proceedings of the eleventh annual symposium on Computational geometry 1995. ACM.

[43] R. Sharma, M. Zeller, V.I. Pavlovic, T.S. Huang, Z. Lo, S. Chu, Y. Zhao, J.C. Phillips, K. Schulten, *Speech/gesture interface to a visual-computing environment.* IEEE CG&A 20 (2000) 29-37.

[44] J.E.Stone, *An efficient library for parallel ray tracing and animation.* (1998).

[45] E. Harder, W. Damm, J. Maple, C. Wu, M. Reboul, J.Y. Xiang, L. Wang, D. Lupyan, M.K. Dahlgren, J.L. Knight, J. Chem. Theory Comput. 12 (2015) 281-296.

[46] W.L. Jorgensen, D.S. Maxwell, J. Tirado-Rives, J. Am. Chem. Soc. 118 (1996) 11225-11236.

[47] W.L. Jorgensen, J. Tirado-Rives, J. Am. Chem. Soc. 110 (1988) 1657-1666.

[48] H.J. Berendsen, J.P. Postma, W.F. van Gunsteren, J. Hermans, *Interaction models for water in relation to protein hydration*, in *Intermolecular forces*. 1981, Springer p.p. 331-342.

[49] A. Otero-de-la-Roza, E.R. Johnson, J. Contreras-García, Phys. Chem. Chem. Phys. 14 (2012) 12165-12172.

[50] E.R. Johnson, S. Keinan, P. Mori-Sanchez, J. Contreras-Garcia, A.J. Cohen, W. Yang, Revealing noncovalent interactions, J. Am. Chem. Soc. 132 (2010) 6498-6506.

[51] *Schrödinger Release 2016-4: Maestro, Schrödinger, LLC, New York, NY, 2016.* 2015.

[52] Clinical and Laboratory Standards Institute (CLSI). Performance standards for antimicrobial susceptibility testing; 16th informational supplement, CLSI M100-S18, 2008, Clinical and Laboratory Standards Institute, Wayne, PA, USA.

[53] M.C. Estrella, A.G. Lpez, A.A. Izquierdo, L.B. Martinez, I.Cuesta, M.J. Buitrago, J.L.R. Tudela, Clinical and Laboratory Standards Institute (CLSI), Reference method for broth dilution antifungal susceptibility testing yeast, approved standard, M27-A3, 2008, Clinical and Laboratory Standards Institute, Wayne, PA, USA.

[54] S.H.R. Sebastian, M.A. Al-Alshaikh, A.A. El-Emam, C.Y. Panicker, J. Zitko, M. Dolezal, C. Van Alsenoy, J. Mol. Struct. 1119 (2016) 188-199.

[55] Y.S. Mary, N.Z. Alzoman, V.V. Menon, E.S. Al-Abdullah, A.A. El-Emam, C.Y. Panicker, O. Temiz-Arpaci, S. Armakovic, S.J. Armakovic, C. Van Alsenoy, J. Mol. Struct. 1128 (2017) 694-706.

[56] S.S. Parveen, M.A. Al-Alshaikh, C.Y. Panicker, A.A. El-Emam, M. Arisoy, O. Temiz-Arpaci, C. Van Alsenoy, J. Mol. Struct. 1115 (2016) 94-104.

[57] A.A. El-Emam, A.S. Al-Tamimi, K.A. Al-Rashood, H.N. Misra, V. Narayan, O. Prasad, L. Sinha, J. Mol. Struct. 1022 (2012) 49-60.

[58] K.S. Resmi, Y.S. Mary, H.T. Varghese, C.Y. Panicker, M. Pakosinska-Parys, C. Van Alsenoy, J. Mol. Struct. 1098 (2015) 130-145.
[59] Z. Karchmarzyk, W. Malinka, X-ray Struct. Anal. 23 (2007) x151-x152.
[60] N.B. Colthup, L.H. Daly, S.E.Wiberly, Introduction of Infrared and Raman Spectroscopy, Academic Press, New York, 1975.
[61] L.J. Bellamy, The Infrared Spectrum of Complex Molecules, third Edn., Chapman and Halls, London, 1975.
[62] Y.S. Mary, H.T. Varghese, C.Y. Panicker, M. Dolezal, Spectrochim. Acta A 71 (2008) 725-730.
[63] N.P.G. Roeges, A Guide to the Complete Interpretation of Infrared Spectra of Organic Structures, John Wiley and Sons, New York, 1994.
[64] R.M. Silverstein, G.C. Bassler, T.C. Morril, Spectrometric Identification of Organic Compounds, fifth ed., John Wiley and Sons Inc., Singapore, 1991.
[65] G. Socrates, Infrared Characteristic Group Frequencies, John Wiley and Sons, New York, 1981.
[66] J.B. Bhagyasree, J. Samuel, H.T. Varghese, C.Y. Panicker, M. Arisoy, O. Temiz-Arpaci, Spectrochim. Acta A 115 (2013) 79-91.
[67] Y.S. Mary, C.Y. Panicker, P.L. Anto, M. Sapnakumari, B. Narayana, B.K. Sarojini, Spectrochim. Acta 135 (2015) 81-92.
[68] G. Varsanyi, Assignments of Vibrational Spectra of Seven Hundred Benzene Derivatives, Wiley, New York, 1974.
[69] S.H.R. Sebastian, A.M.S. Al-Tamimi, N.R. El-Brollosy, A.A. El-Emam, C.Y. Panicker, C. Van Alsenoy, Spectrochim. Acta A 134 (2015) 316-325.
[70] Y.S. Mary, C.Y. Panicker, M. Sapnakumari, B. Narayana, B.K. Sarojini, A.A. Al-Saadi, C. Van Alsenoy, J.A. War, Spectrochim. Acta A 136 (2015) 483-493.
[71] Y.S. Mary, C.Y. Panicker, M. Sapnakumari, B. Narayana, B.K. Sarojini, A.A. Al-Saadi, C. Van Alsenoy, J.A. War, H.K. Fun, Spectrochim. Acta A 136 (2015) 473- 482.
[72] D. Nemeckova, Y.S. Mary, C.Y. Panicker, H.T. Varghese, C. Van Alsenoy, M. Prochazkova, P. Pazdera, A.A. Al-Saadi, J. Mol. Struct. 1094 (2015) 210-236.
[73] R. Renjith, Y.S. Mary, C.Y. Panicker, H.T. Varghese, M. Pakosinska-Parys, C. Van Alsenoy, A.A. Al-Saadi, Spectrochim. Acta 129 (2014) 438-450.
[74] H.L. Spell, Anal. Chem. 41 (1969) 902-905.
[75] M.A.S. da Silva, S. Pinheiro, T. Francisco, F.O.N. Da Silva, A.A. Batista, J. Ellena, I.M.M. Varvalho, J.R. de Sousa, F.A. Dias-Filho, E. Longhinotti, I.C.N. Diogenes, J. Braz. Chem. Soc. 21 (2010) 1754-1759.
[76] A.B. Ahmed, H. Feki, Y. Abid, H. Boughzala, C. Minot, A. Mlayah, J. Mol. Struct. 920 (2009) 1-7.
[77] H.O. Kalinowski, S. Brawn, Carbon13 NMR Spectroscopy, John Wiley and Sons, Chichester, 1988.
[78] Martin, R.L., J.Chem. Phys. 118 (2003) 4775-4777.
[79] T. Le Bahers, C. Adamo, I. Ciofini, J. Chem.Theo. Comp. 7 (2011) 2498-2506.
[80] C.A. Guido, P. Cortona, B. Mennucci, C. Adamo, J. Chem.Theo. Comp. 9 (2013) 3118-3126.
[81] E.D. Glendening, A.E. Reed, J.E. Carpenter, F. Weinhold, NBO Version 3.1, Gaussian Inc., Pittsburgh, PA, 2003.
[82] K. Fukui, Theory of Orientation and Stereoselections, Springer-Verlag, New York, 1975.

[83] V.V. Menon, E. Fazal, Y.S. Mary, C.Y. Panicker, S. Armakovic, S.J. Armakovic, S. J. Mol. Struct. 1127 (2017) 124-137.
[84] A.H. Pandith, N. Islam,PLoS ONE 9 (2014) e114125.
[85] R.P. Verma, C. Hansch, Bioorg. Med. Chem. 13 (2005) 2355-2372.
[86] K. Srivastava, A. Srivastava, P. Tandon, K. Sinha, J. Wang, J. Mol. Struct. 1125 (2016) 751-762.
[87] Y.S. Mary, H.T. Varghese, C.Y. Panicker, M. Girisha, B.K. Sagar, H.S. Yathirajan, A.A. Al-Saadi, C. Van Alsenoy, Spectrochim. ActaA 150 (2015) 543-556.
[88] C. Adant, M. Dupuis, J.L. Bredas, Int. J. Quantum Chem. 56 (1995) 497-507.
[89] Y.S. Mary, C.Y. Panicker, H.T. Varghese, K. Raju, T.E. Bolelli, I. Yildiz, C.M. Granadeiro, H.I.S. Nogueira, J. Mol. Struct. 994 (2011) 223-231.
[90] A. Chandran, H.T. Varghese, C.Y. Panicker, C. Van Alsenoy, G. Rajendran, J. Mol. Struct. 1001 (2011) 29-35.
[91] J.A. War, K. Jalaja, Y.S. Mary, C.Y. Panicker, S. Armakovic, S.J. Armakovic, S.K. Srivastava, C. Van Alsenoy, J. Mol. Struct. 1129 (2017) 72-85.
[92] J.S. Murray, J.M. Seminario, P. Politzer, P. Sjoberg, Int. J. Quantum Chem. 38 (1990) 645-653.
[93] P. Politzer, F. Abu□Awwad, J.S. Murray, Int. J. Quantum Chem. 69 (1998) 607-613.
[94] F.A. Bulat, A. Toro-Labbé, T. Brinck, J.S. Murray, P. Politzer, J. Mol. Model. 16 (2010) 1679-1691.
[95] P. Politzer, J.S. Murray, F.A. Bulat, J. Mol. Model. 16 (2010) 1731-1742.
[96] A. Michalak, F. De Proft, P. Geerlings, R. Nalewajski, J. Phys. Chem. A, 103 (1999) 762-771.
[97] X. Ren, Y. Sun, X. Fu, L. Zhu, Z. Cui, J. Mol. Model. 19 (2013) 2249-2263.
[98] L.-L.Ai, J.-Y. Liu, J. Mol. Model. 20 (2014) 1-10.
[99] W. Sang-Aroon, V. Amornkitbamrung, V. Ruangpornvisuti, J. Mol. Model. 19 (2013) 5501-5513.
[100] J. Kieffer, É. Brémond, P. Lienard, G. Boccardi, J. Mol. Struct. THEOCHEM, 954 (2010) 75-79.
[101] S.W. Hovorka, C. Schöneich, Oxidative degradation of pharmaceuticals: Theory, mechanisms and inhibition, J. Pharm. Sci. 90 (2001) 253-269.
[102] K.A. Connors, G.L. Amidon, and V.J. Stella, *Chemical stability of pharmaceuticals: a handbook for pharmacists*. 1986: John Wiley & Sons.
[103] D. Johnson, L. Gu, Encyclopedia of pharmaceutical technology 1 (1988) 415-449.
[104] J.S. Wright, H. Shadnia, L.L. Chepelev, J. Comput. Chem. 30 (2009) 1016-1026.
[105] G. Gryn'ova, J.L. Hodgson, M.L. Coote, Org. Biomol. Chem. 9 (2011) 480-490.
[106] T. Andersson, A. Broo, E. Evertsson, J. Pharm. Sci. 103 (2014) 1949-1955.
[107] R.V.Vaz, J.R. Gomes, C.M. Silva, J. Supercritic. Fluids, 107 (2016) 630-638.
[108] I.V. Tetko, V.Y. Tanchuk, J. Chem.Inf. Comp. Scie. 42 (2002) 1136-1145.
[109] I.V. Tetko, V.Y. Tanchuk, and A.E. Villa, J. Chem.Inf. Comp. Scie. 41 (2001) 1407-1421.
[110] I.V. Tetko, V.Y. Tanchuk, T.N. Kasheva, A.E. Villa, J. Chem.Inf. Comp. Scie. 41 (2001) 1488-1493.
[111] I.V.Tetko, G.I. Poda, J.Med. Chem. 47 (2004) 5601-5604.
[112] I.V. Tetko, P. Bruneau, J. Pharm.Scie. 93 (2004) 3103-3110.

[113] G. Poda, I. Tetko. *Towards predictive ADME profiling of drug candidates: Lipophilicity and solubility*. in Abstracts of papers of The American Chemical Society. 2005. Amer. Chemical. Soc. 1155 16th St, NW Washington, D.C. 20036 USA.

[114] A.K. Ghose, V.N. Viswanadhan, J.J. Wendoloski, J. Comb.Chem. 1 (1999) 55-68.

[115] I. Moriguchi, S. Hirono, L. Qian, I. Nakagome, Y. Matsushita, Chem.Pharm. Bull. 40 (1992) 127-130.

[116] C.A. Lipinski, F. Lombardo, B.W. Dominy, P.J. Feeney, Adv. Drug Deliver Rev. 23 (1997) 3-25.

[117] C.A. Lipinski, Drug Disc. Today: Techno. 1 (2004) 337-341.

[118] D.F. Veber, S.R. Johnson, H.-Y. Cheng, B.R. Smith, K.W. Ward, K.D. Kopple, J Med.Chem. 45 (2002) 2615-2623.

[119] M. Congreve, R. Carr, C. Murray, H. Jhoti, Drug Discov. Today 8 (2003) 876-877.

[120] A.K. Ghose, V.N. Viswanadhan, J.J. Wendoloski, J. Phys. Chem. 102 (1998) 3762-3772.

[121] A. Lagunin, A. Stepanchikova, D. Filimonov, V. Poroikov, Bioinformatics 16 (2000) 747-748.

[122] Muscular Dystrophy: Causes, symptoms and treatments written by T.Newmann, Medical news letters, Reviewed by University of Illinois, Chicago, School of MedicineKnowledge,centre, **www.medicalnewstoday.com/articles/187618**.

[123] M.C. Botfield, O. Eckard, D.J. Lauffer, Piperazine and piperidine derivatives for treatment of neurological diseases, PCT/US2003/031080, WO2004031148A1, 2005.

[124] J. Inoue, Y. Yoshida, Y.-S.Cui, M. Azuma, Piperazine derivatives and use of the same, PCT/JP1996/001884, WO 1997003060 A1, 1997.

[125] J.M. Squire, H.A. Al-Khayat, C. Knupp, P.K. Luther, Advan. Protein Chem. 71 (2005) 17-87.

[126] L. Tskhovrebova, J. Trinick, Nature Rev. Mol. Cell. Biol. 4 (2003) 679-689.

[127] S. Lange, E. Ehler, M. Gautel, Trends Cell Biol. 16 (2006) 11-18.

[128] L. Tskhovrebova, J. Trinick, J. Biol. Chem. 279 (2004) 46351-46354.

[129] S. Müller, S. Lange, M. Gautel, M. Wilmanns, J. Mol. Bio. 371 (2007) 469-480.

[130] O. Trott, A. J. Olson, J. Comput. Chem. 31 (2010) 455-461.

[131] B. Kramer, M. Rarey, T. Lengauer, PROTEINS: Struct. Funct.Genet. 37 (1999) 228-241.

- Novel benzoxazole derivative was characterized by IR and Raman spectroscopy,
- Study of antimicrobial activity indicates potential for practical applications of PMPEPAB
- DFT calculations revealed the most important reactive centers,
- MD simulations were used in order to investigate reactivity with water molecules,
- Docking study revealed significant binding properties against 2J8O protein.